Engineering Structures 262 (2022) 114341

Contents lists available at ScienceDirect

Engineering Structures

journal homepage: www.elsevier.com/locate/engstruct

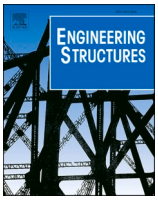

Analysing local failure scenarios to assess the robustness of steel truss-type bridges

Giacomo Caredda [a], M. Cristina Porcu [b], Manuel Buitrago [a,*], Elisa Bertolesi [c], José M. Adam [a]

[a] ICITECH, Universitat Politècnica de València. Camino de Vera s/n, 46022 Valencia, Spain
[b] University of Cagliari, Department of Civil and Environmental Engineering and Architecture, Piazza d'Armi, 09123 Cagliari, Italy
[c] Department of Civil and Environmental Engineering, Brunel University London, UB8 3PH Uxbridge, UK

ARTICLE INFO

Keywords:
Alternative Load Paths
Computational modelling
Recommendations
Robustness
Steel truss-type bridges

ABSTRACT

Many of the steel bridge collapses occur in truss-type bridges. This is, in fact, the focus of this study involving an assessment of the robustness of this type of structures based on an actual bridge that the authors had extensively monitored and controlled. Robustness was assessed by means of computer simulations of various Damage Scenarios (DSs) to analyse the structural bridge capacity to efficiently activate Alternative Load Paths (ALPs). The computational models have been previously validated with the results of load tests on the bridge and a laboratory test on a full-scale bridge span. The DSs have considered a series of non-simultaneous failures in different elements. The results indicate that the structure is capable of not triggering a disproportionate collapse after each of the DSs with the help of the efficient activation of ALPs that required the contribution of other elements with extra-strength capacity as well as from the superstructure and the joints working under bending moments. The results were used as the basis for practical recommendations for: i) the design of new steel bridges and the retrofit of existing ones and ii) monitoring the structure for the optimal position of sensors to predict local failures that could spread to the rest of the bridge.

1. Introduction

Bridges over the Firth of Tay (Scotland, 1879), the Birz river (Switzerland, 1891), the Peene river (Germany, 1900) and the the Quebec bridge (Canada, 1907), or the Seongsu bridge (South Korea, 1994), the I-35 bridge in Minneapolis (USA, 2007), the Chauras bridge (India, 2012) and the I-5 Skagit River in Washington (USA, 2013), are some historic and recent examples of the disproportionate collapse of truss-like railway and road bridges, characterized by a huge number of deaths, injuries and serious economic losses [1–4]. A study made in the US [5] identified more than 500 steel truss-type bridge failures in a period of 11 years (1989–2000), showing that they occur frequently (an average of 9.7 bridges a year in the US) and therefore such bridges are highly vulnerable. Natural disasters, impacts, overloads, structural and design deficiencies, construction and supervision mistakes or insufficient maintenance/inspection are the main causes of these collapses. A common feature is that a local failure sets off the progressive collapse of the entire structure or at least a great part of it.

While the research on progressive building collapse is quite extensive [6–10] this cannot be said for bridge structures [1,11–17], in which case most studies deal with actual cases and few with experimental, numerical or theoretical studies. In this field there is still a long way to go in the study of bridge structural behaviour after a local failure [18] as well as compiling practical recommendations for robust designs and existing bridge monitoring. The latest international standards [19–21] are oriented to aid in the design and construction of robust structures. All of them include Alternative Load Paths (ALPs) that can be activated after the local failure of an element. This approach through ALPs follows the scenario-independent approach and does not deal with the causes of the failure but only aims at minimizing the consequences that a local failure may produce in the rest of the structure.

In view of the vulnerability of truss-type bridges and the low number of studies published on progressive bridge collapses, the present study is aimed at performing a complete robustness assessment of this type of structures considering several local failure scenarios, in order to: (i) assess the activation of possible ALPs, (ii) study the structural performance and resistant capacity after activating these ALPs, and (iii) suggest recommendations for designing robust bridges and for controlling those already existing. The subject of this study is included in the aims of the Cluster 3 of the Horizon Europe Program (Civil Security for Society),

* Corresponding author.
E-mail address: mabuimo1@upv.es (M. Buitrago).

https://doi.org/10.1016/j.engstruct.2022.114341
Received 14 December 2021; Received in revised form 21 April 2022; Accepted 27 April 2022
Available online 14 May 2022

Fig. 1. Bridge view from a drone.

in a Sustainable Development Goal (Goal 9: Build resilient infrastructure, promote sustainable industrialization and foster innovation) and in the targets of the Sendai Framework.

After the Introduction, Section 2 presents a description of the real case used to carry out the numerical study and summarizes the underpinning work of this study. Section 3 describes the computational simulation together with a description of the Finite Element (FE) model, the loads considered and the validation process. Section 4 contains the main results of the robustness assessment for every defined local damaged scenario. Section 5 contains a discussion of the results obtained with conclusions common to all the failure scenarios and gives practical recommendations. Finally, Section 6 provides a summary of the conclusions.

2. Description of the bridge and previous work

This section is devoted to the description of a real case used as a reference structure to carry out a robustness analysis of steel truss-type railway bridges. This real case is located in Eastern Spain which was lab and tested in the field by some of the authors of this article in previous work [16,22,23]. Currently, this bridge is also real-time monitored by some of the authors with more than 250 sensors and within the Structural Health Monitoring (SHM) discipline. Since the authors are familiar with it from an experimental point of view, the adopted real case was a unique opportunity to perform a computational study.

2.1. Geometry

The bridge is a Pratt-type steel structure built in 1913–1915 and made with riveted connections (see Fig. 1). The structural scheme of the bridge is composed of six spans organized symmetrically in four lateral isostatic structures and a statically indeterminate central structure composed of two spans. Five steel columns with variable heights and two lateral abutments complete the geometry of the bridge which is approximately 170 m long with spans lengths and depths varying from 21 m to 42 m and from 2.3 m to 4.0 m, respectively, span widths of 2.8 m and only one traffic lane. The reader is referred to references [16,22] for further details on the bridge geometry. One of the isostatic spans was selected for the present study since it is currently closely monitored and has been lab-tested.

2.2. Summary of the experimental results

In this section, the experimental results obtained from the ongoing real-time structural health monitoring of the bridge are discussed. For the selected isostatic span, the first natural mode was recorded using monoaxial accelerometers installed on the upper deck of the bridge mid span. OMA identification of this span showed that the structure has a fundamental frequency of 8.9 Hz, corresponding to the first bending mode. The dynamic response under operational conditions was monitored by fibre optic strain sensors in different elements, including a column, a transversal beam and a lower chord that were selected to

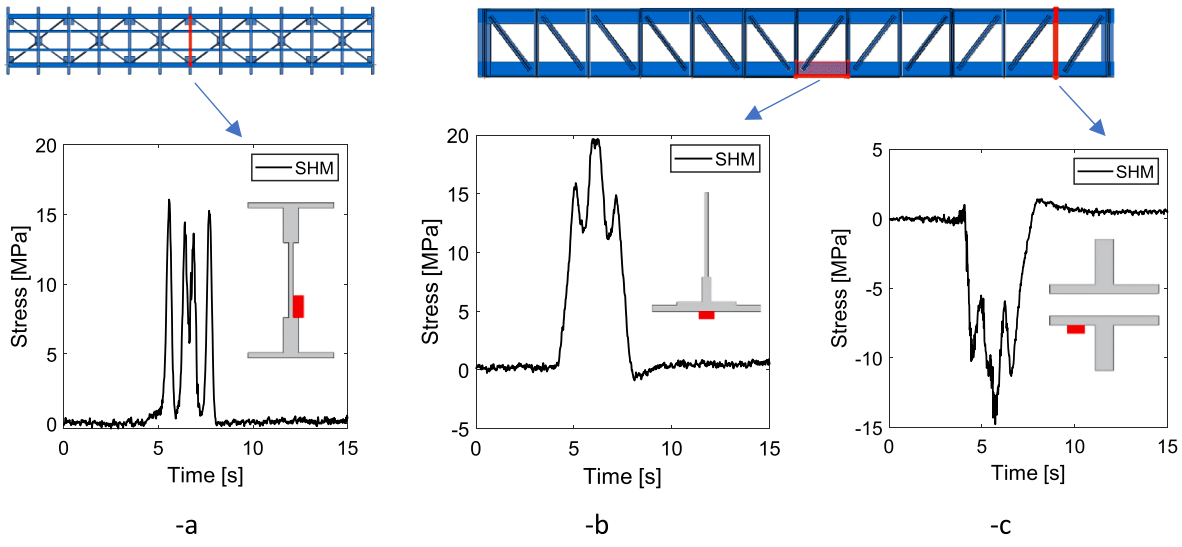

Fig. 2. Fibre Optic sensor readings from SHM: cross beam (-a), lower chord (-b) and column (-c).

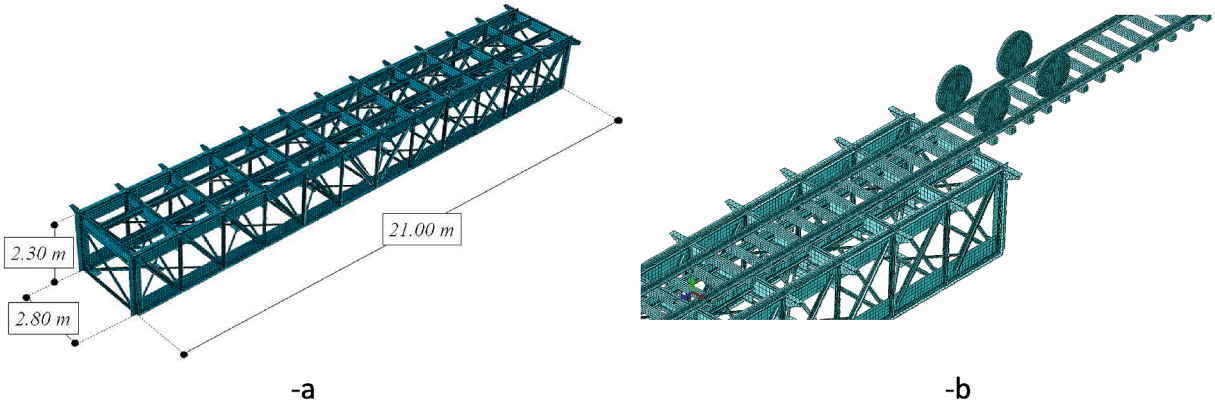

Fig. 3. 3D model of the bridge: adopted discretization (-a) and detail of the axle configuration (-b).

represent the whole structure and to validate the FE model. The relevant results (obtained by multiplying strain readings of a train passing over the bridge by Young's Steel Modulus equal to 210GPa) in terms of stress reading histories from sensors of one reference passing train are shown in Fig. 2.

3. Computational modelling

3.1. Detailed Finite element model

The Finite Element (FE) model of one isostatic span of the bridge was modelled in Abaqus [24]. Fig. 3 depicts the 3D geometry of the bridge with the adopted mesh (see Fig. 3-a) and a detail of the axle configuration used to impose the train loads (see Fig. 3-b). The whole model comprised approximately 500,000 3D first-order solid (continuous) 8-noded finite elements using a fully integration scheme to discretize the bridge structure. This high number of FEs was necessary to perfectly reproduce the geometry and connections of the elements composing the structure.

The level of detail attained in the present work represents a good compromise to study the bridge response and stress transfer among the different elements, simplifying the interactions at the level of the riveted connections, which were not modelled. In agreement with the field observations, passing train was expected to produce stress increases in the main elements of the structure during normal operational conditions to within 40% of the steel yielding strength. After in situ measurements, material mechanical tests and a modal identification procedure the authors considered a Young's Modulus of 210 GPa, Poisson ratio of 0.3 and density of 7850 kg/m^3 for the steel elastic behaviour. The boundary conditions were selected idealizing the real restraints observed in the structure, which was assumed to behave as a simply-supported bridge span. The boundary conditions were applied by restricting the corresponding DOFs at the two ends of the bridge model to simulate the roller and pinned supports. The internal elements are fully connected to each other this being the most appropriate assumption based on numerical-experimental results the authors obtained in past studies [16,22]. The passing train was simulated statically with equivalent forces resembling those distributed by the train wheels on the rails and underlying structural members. Thus, the model included both sleepers and rails, which were simulated as independent elements perfectly connected to each other. In agreement with common practice, these elements were supposed to be completely fixed to the underlying structure while the loading system comprised the application of movable static forces directly on the rails (see Fig. 3-b). Introducing the rails in the model made it possible to consider the wheel-rail interaction with surface-to-surface contacts. The sleepers worked as rail support points and both rails and sleepers were essential as they could be the final line of defence in some local failures.

3.2. Traffic loads

A railway train with an assigned axle configuration was adopted to represent the actual traffic loading on the bridge. As the robustness assessment was performed under accidental loading situations, the real loading conditions were not increased by any safety factor. The train's axle spacings and weights are provided in Fig. 4-a, while Fig. 4-b shows a scheme of the train-structure interaction. The train was treated as lumped masses placed over different axles and finally imposed on the bridge structure by means of general contact interactions between wheels and rails. The train was considered to be fully-loaded during the simulations (see Fig. 4-a).

3.3. Validation

The FE model was validated with different approaches. The first approach was based on the results obtained experimentally with the OMA identification from the SHM sensors monitoring the bridge. The model comprised the self-wight of the structure and the material

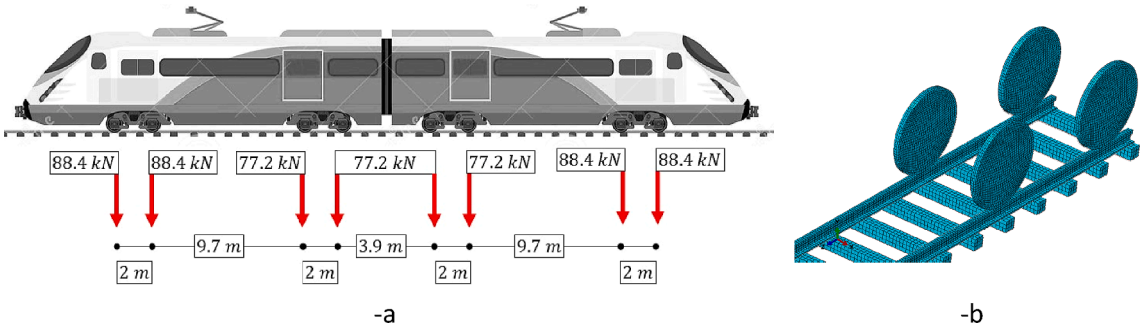

Fig. 4. Train-structure interaction: adopted axle spacings and weights (-a) and wheel-rail interaction(-b).

Table 1
Fundamental modes and frequencies.

	Mode	Frequency	Sketch
Mode 1	1st lateral bending	8.83 Hz	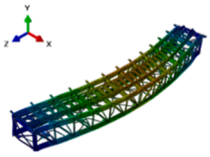
Mode 2	Vertical bending	9.07 Hz	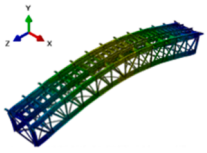
Mode 3	Torsional	14.45 Hz	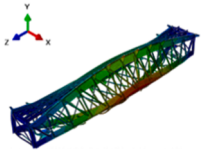
Mode 4	2nd lateral bending	18.77 Hz	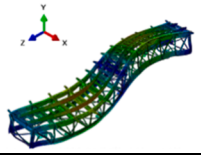

properties described in Section 2 and was firstly studied by modal analysis for the identification procedure (see Table 1). As it can be seen, the structure's vertical bending mode was attained at a frequency of 9.07 Hz, which is close to the real one (8.90 Hz). The modal analysis also estimated other natural frequencies and relevant modes, which involved: a lateral bending mode at 8.83 Hz, a torsional mode at 14.45 Hz and a 2nd lateral bending mode at 18.77 Hz.

The second approach was carried out taking into account the structural response of the bridge in operational condition. The stress increases produced by a passing train on some structural elements of the bridge were monitored by the sensors. The sensor readings were compared to the numerical outputs without considering the bridge self-weight and scaling the static numerical time-steps to be consistent with the considered train velocity (39 km/h). Fig. 5 shows the stress evolution on different structural elements and how the FE model accurately reproduces the real response of the structure.

4. Robustness

This section presents a robustness assessment of the bridge comprising different damage scenarios (DS) and analyses of the bridgés structural response. The DS nomenclature was defined as X-N-Z where: X is the type of element (i.e., LC, UC, D, C, UT and US standing for lower chord, upper chord, diagonal, column, upper transversal beam, and upper stringer, respectively); N is the element number; and Z is the side (i.e., L and R for left or right, respectively). This nomenclature was used for all the DS elements except for transversal beams, where the side Z is not relevant. A sketch of the adopted nomenclature is provided In Table 2.

In this study, the damage was simulated through the removal of the involved element from the model, which implied the assumption of a local failure. Steel elements may be in fact affected by different types of damage, the detailed modelling of which typically requires dedicated analysis involving damage evolution and propagation. A detailed level of modelling is however rarely necessary, while the presence of damage is often introduced in numerical models through simpler assumptions, like for instance the reduction of the element stiffness according to the damage severity [25]. A complete failure of the element can simulate the case of a brittle fracture due to a fatigue crack, a loss of the connection, a blast, or an impact, as observed in [26]. Regardless of the nature of the damage-initiating hazard, however, the assumption of a sudden removal of the damaged elements is an effective way to evaluate the ability of the system to resist a cascading event and thus to study its robustness. The approach of the sudden removal of the damaged element was in fact followed by other authors to study the progressive collapse of buildings [27] or the dynamic reliability of truss bridges [28].

4.1. Damage scenarios (DSs)

A group of six damage scenarios was considered in the study in the form of sudden local failures. The DSs are summarized in Table 2 organized according to the type of element damaged during the simulation (i.e., primary, for transversal beams and stringers, or secondary elements for elements belonging to the Pratt-type structure). Each DS is provided with a sketch showing the position of the removed element along the bridge. Each simulation was performed considering both undamaged and damaged scenarios (the latter achieved by removing the entire element from the model) and evaluating the difference in terms of global deflection and stress increases at some characteristic points over the structure. As the failure of a chord implies the unloading of the diagonal connected to it, in both sequences LC6L and UC6L, diagonal D6L was removed together with the lower or upper chord, respectively.

A preliminary study of the numerical stress contours relevant to the passage of the train over the undamaged structure allowed to choose six damage scenarios involving some of the most demanded primary or secondary elements of the bridge. Owing to the role of such elements in the performance of the bridge, the six considered DSs can be taken as the

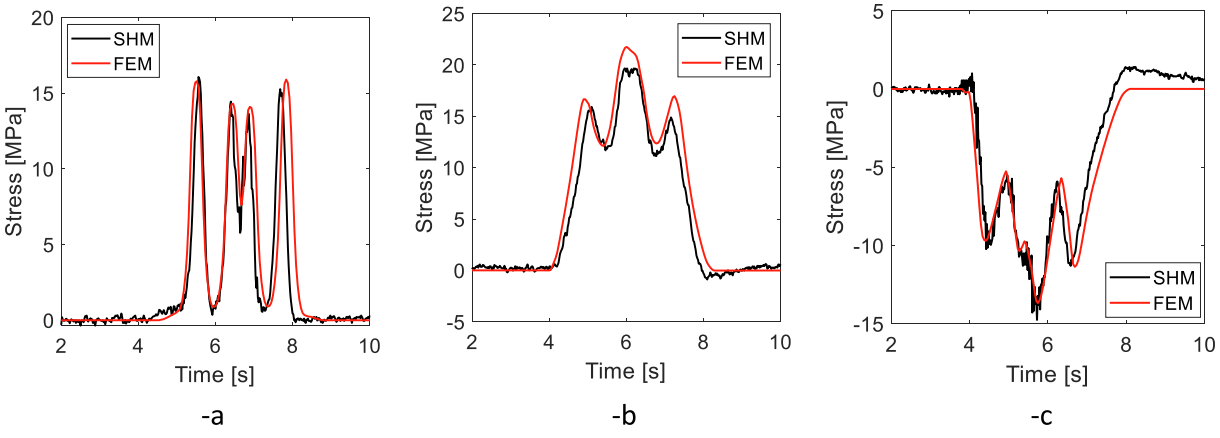

Fig. 5. Comparison of fibre optic sensor readings from SHM and FE results: transversal beam (-a), lower chord (-b) and column (-c).

Table 2
Nomenclature and Damage Scenarios (DSs).

Nomenclature

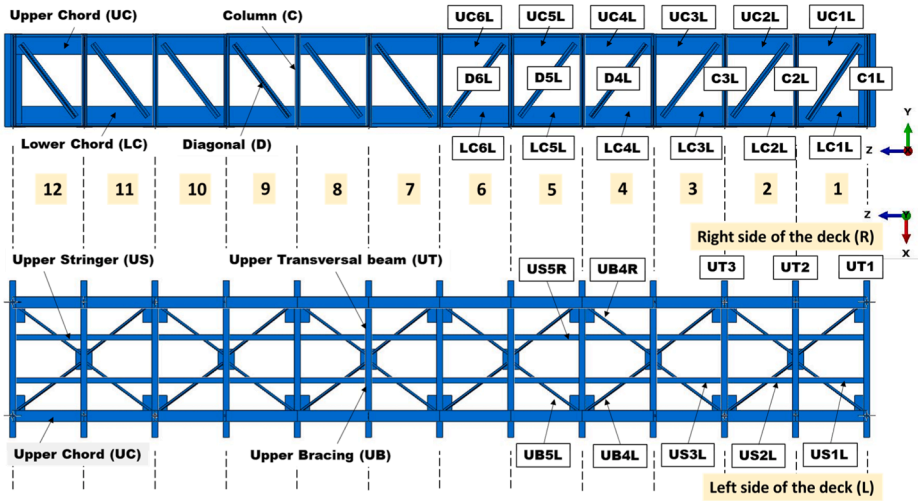

Sub-Groups	Damage Sequence	Sketch
PE - Primary Elements	UT7	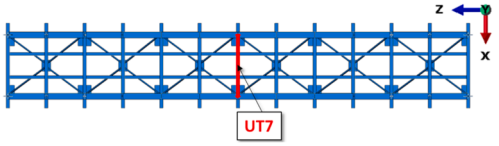
	US6L	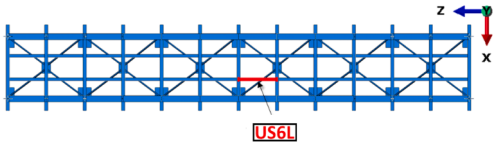
SE - Secondary Elements	LC6L	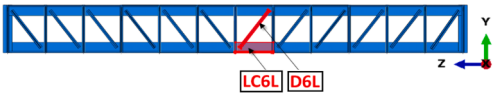
	UC6L	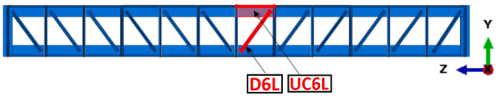
	D3L	
	C2L	

most representative for the assessment of the bridge's robustness. It is to note that the considered DSs involved only elements belonging to a half part of the bridge and to its left side. Due to structural symmetry, however, they are representative of any DSs involving specular elements with respect to the longitudinal and transversal axes of the bridge.. The group of considered DSs thus included a complete robustness assessment of the bridge. The main results obtained for the considered DSs are discussed in the following sections.

4.2. Structural response of the bridge: Primary elements (PE)

4.2.1. Damage scenario DS-UT7

Relevant to the DS-UT7 damage scenario (Table 2), two close-up views of the stress contours are shown in Fig. 6, both taken in a time-step in which the axles of the train are centred over the bridge span considering the undamaged and damaged scenario. This time step was selected to compare the stress contours since it is the most loaded situation of the isostatic span and is useful for the study of the secondary elements.

Very slight changes in the stress distribution can be noted by comparing these contour maps. More information about local stress changes and transfer mechanisms can be taken from a local analysis of the stress histories, as it will be done in the following. The deformed shape and the vertical displacement contour maps of the undamaged and damaged scenarios are provided in Fig. 7, both taken in the same time-step in Fig. 6. No increase of the maximum vertical displacement d_{ymax} was observed after the element's removal. As expected, the removal of the transversal beam UT7 did not significantly affect the bridge's global stiffness and consequently not even its main frequencies and modes. This is shown by the comparison between the first four frequencies and modes presented in Table 3, where the frequency variation in percentage is also provided (the positive or negative signs meaning an increase or reduction of the damaged frequency, respectively). Although the frequency values of the damaged are different from

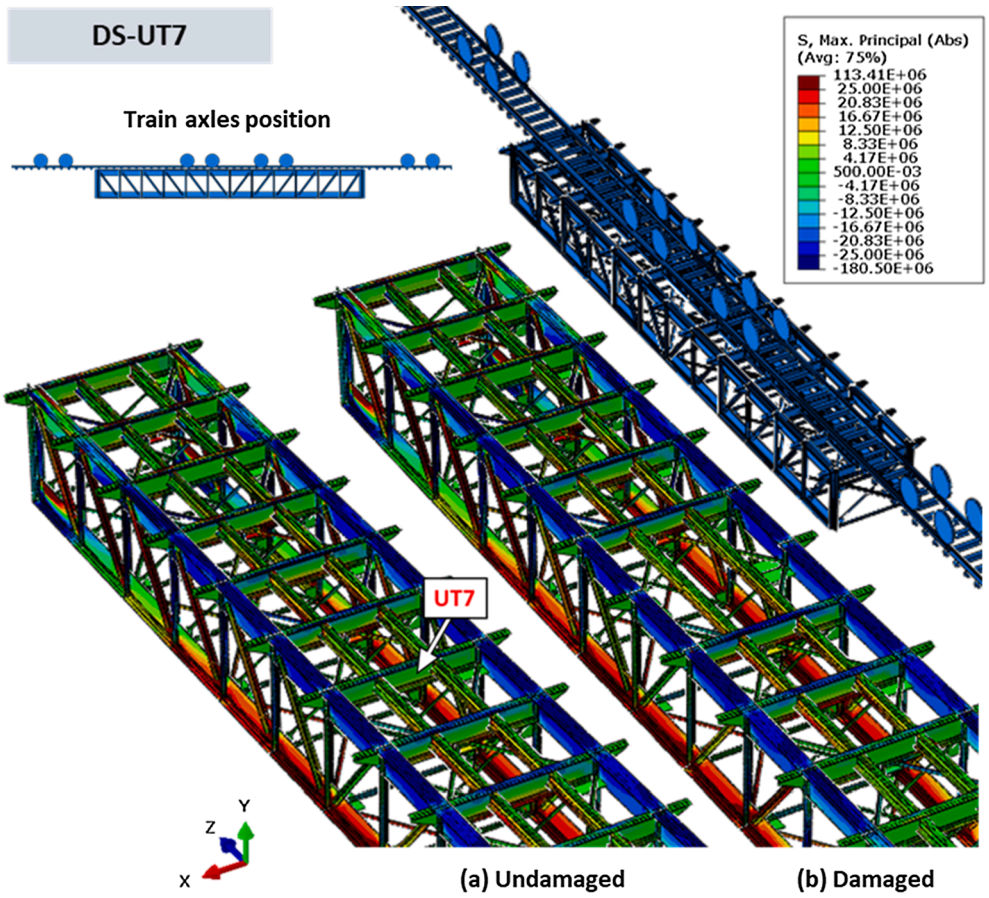

Fig. 6. DS-T7: Principal stress contour maps obtained considering initial undamaged (a) and damaged (b) states. Units in Pa.

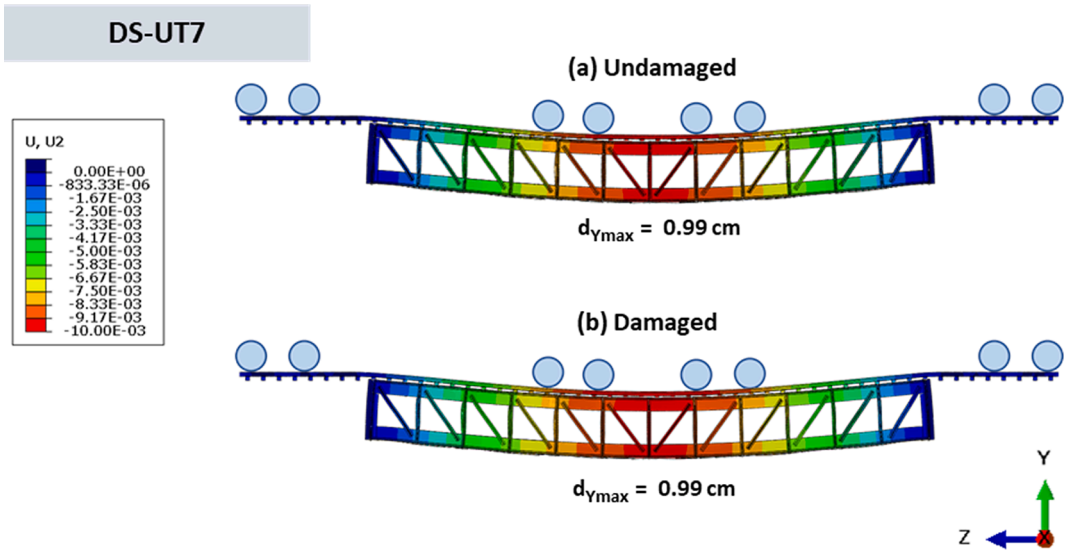

Fig. 7. DS-UT7: Vertical displacement contour maps considering both undamaged (a) and damaged (b) states. Legend units in m.

those of the undamaged structure, the difference is so small (well below 1%) that it is insignificant in terms of global behaviour of the system. Whilst lower natural frequencies typically characterize a damaged structure, a slight increase in the first three frequencies was found in this case. This is not surprising, since it was due to the reduction of the total mass after the removal of the element, which is not compensated enough by the global stiffness reduction. However, it can be noted that removing the damaged element does not limit the validity of this parametric study, since very similar results in terms of global behaviour of the structure would have been found if the mass of the damaged element had been left in the model.

To locally study the effect of removing UT7 from the structure, the stress evolution during the train passage was monitored in two primary elements adjacent to UT7, where a stress transfer mechanism was expected to be activated after the damage.

Fig. 8-a and -b presents the principal stress histories at two points.

Table 3
DS-UT7: First four frequencies and modes for the undamaged and damaged scenarios.

	Undamaged		Damaged (DS-UT7)		Δ (%)
	Mode	freq (Hz)	Mode	freq (Hz)	
Mode 1	1st lateral bending	8.83	1st lateral bending	8.87	0.45
Mode 2	Vertical bending	9.07	Vertical bending	9.12	0.55
Mode 3	Torsional	14.45	Torsional	14.48	0.21
Mode 4	2nd lateral bending	18.77	2nd lateral bending	18.68	−0.48

The first on the transversal beam UT6, adjacent to that removed, the other on the middle-span stringer element US6L. It is worth remembering that both elements are subject to bending actions caused by the train acting directly on the rails, which in turn transmit the external actions to the underlying elements through the sleepers. The identification of the monitoring points was thus carried out paying attention to the stress state of the considered elements. Consequently, a point placed in the lowest cross-section part of both transversal beam UT7 and stringer US6L was selected. The monitoring point was located where the maximum stress occurs, this point not necessarily being the same in the undamaged and damaged conditions. On average, the damage caused a maximum increase in stresses of up to 23% in the adjacent transversal beam UT6, and up to 13% in stringer US6L, where the stresses also switched from tension to compression at certain times, although very low levels of compression stresses were achieved.

The impact of this DS on the rail superstructure was also assessed. A comparison between the time-histories of the vertical displacements experienced by the rail before and after damage are provided in Fig. 8c and 8d, with reference respectively to two monitoring points over the UT7 beam and the US6L stringer. The diagrams show that the rail deflection increased by up to 22 % at the first point and 10% at the second, with a peak of 10.5 mm. The maximum stresses in the rail are comparatively low, with a maximum value of about 32 MPa in the undamaged condition and 52 MPa after damage, with an increase of 63%.

4.2.2. *Damage scenario DS-US6L*

The same analysis carried out in DS-UT7 was carried out considering the removal of the stringer US6L. In this case the element removal produced an asymmetrical bridge asset with an expected impact on the stress transfer mechanism to the undamaged elements, and on the deformed shape.

Consistently with the previous damage scenario and for only the study of the secondary elements, the stress evolutions were tracked considering a specific time-step in which the train is at the centre of the bridge span. The main FE results in terms of stress contour maps considering both undamaged and damaged states are depicted in Fig. 9-a and -b, respectively. A comparison between these maps shows no

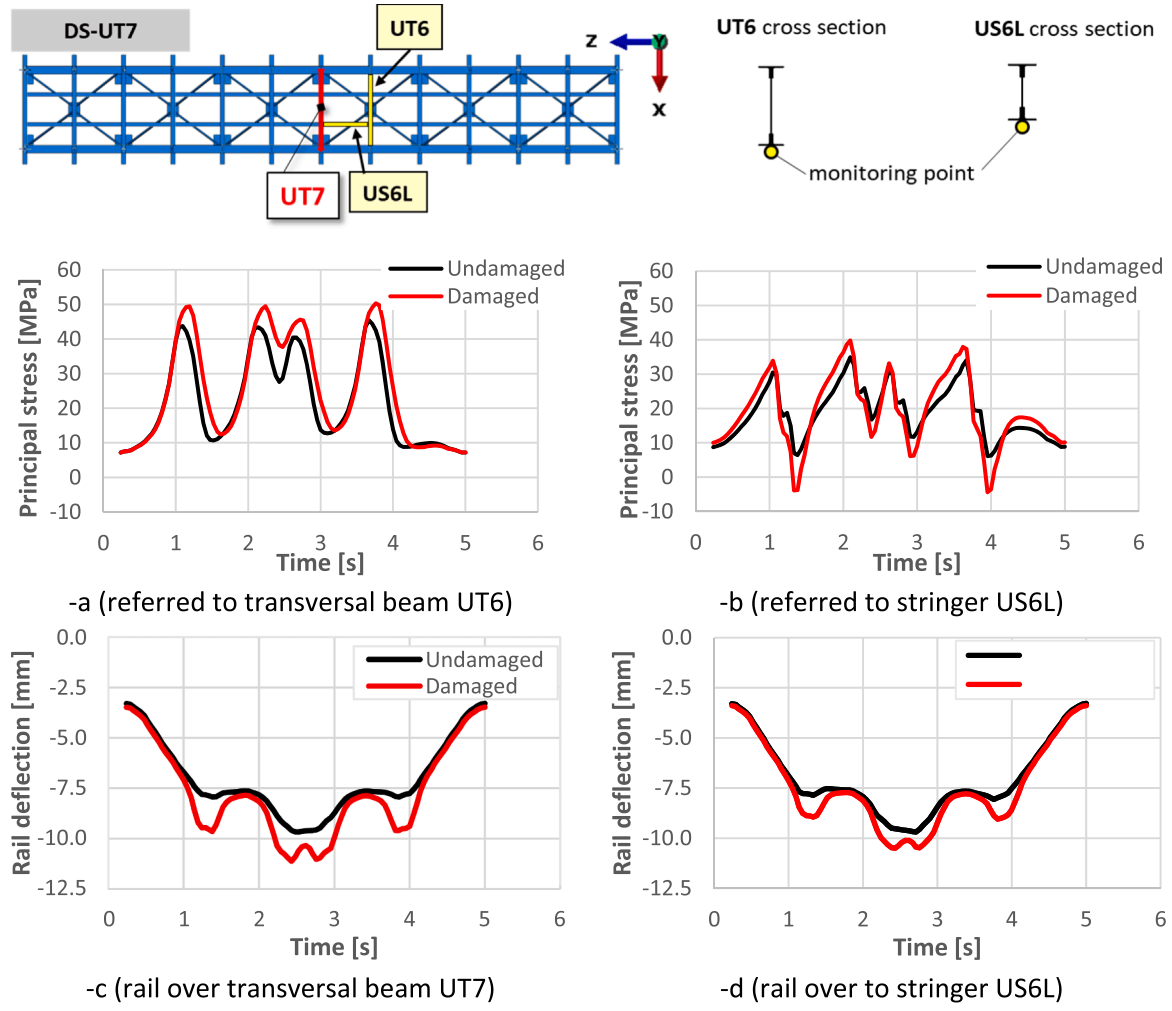

Fig. 8. DS-UT7: Principal stress histories monitored on the transversal beam UT6 (-a) and on the stringer US6L (-b) considering both undamaged and damaged states. Deflection of the rail over beam UT7 (c) and stringer US6L (d).

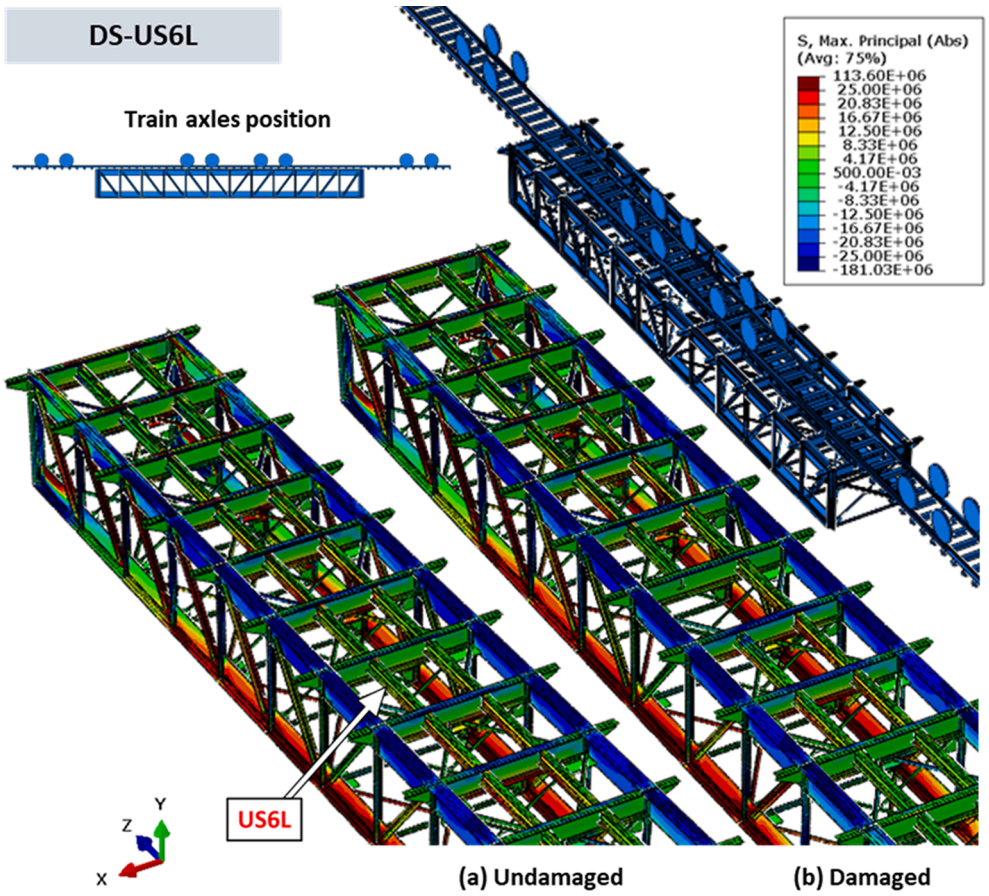

Fig. 9. DS-US6L: Principal stress contour maps obtained considering undamaged (a) and damaged (b) states. Units in Pa.

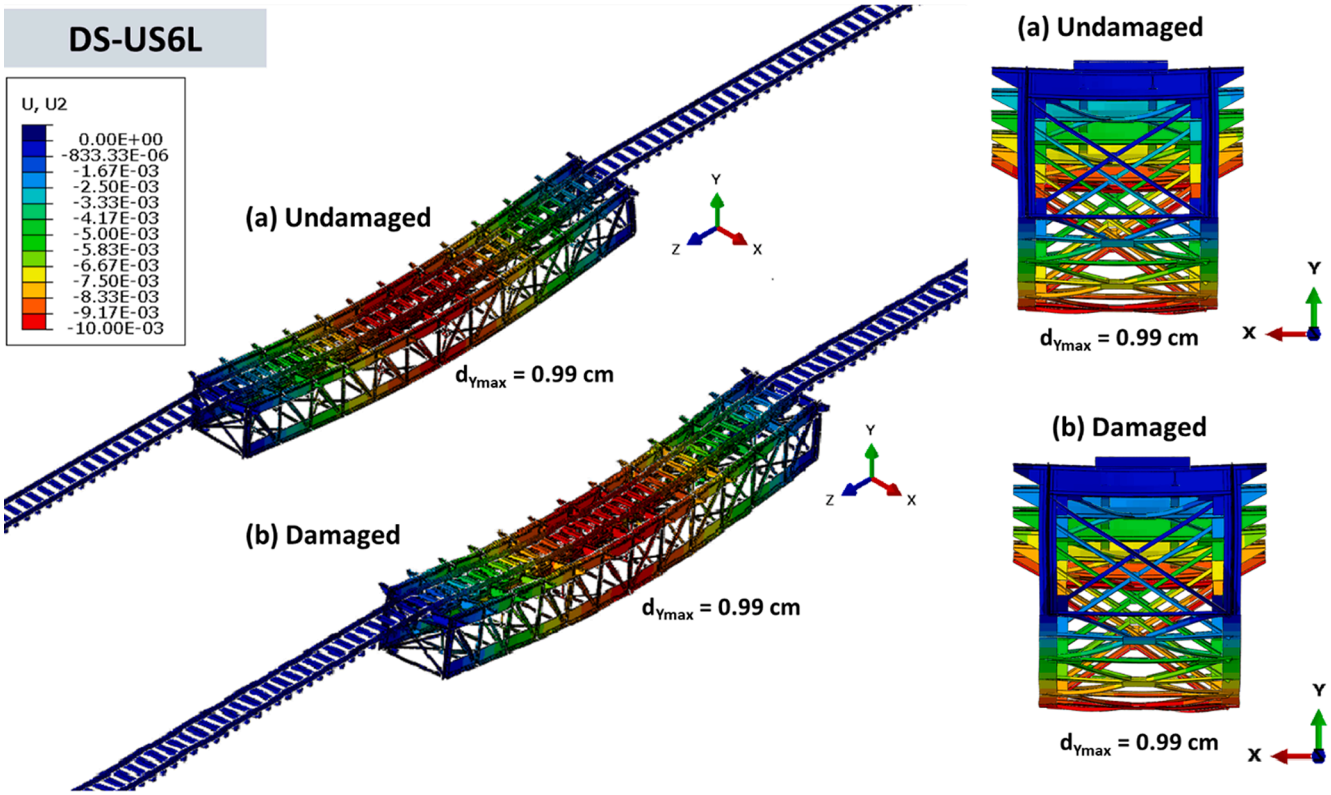

Fig. 10. DS-US6L: Vertical displacement contour maps considering both undamaged (a) and damaged (b) states. Legend units in m.

Table 4
DS-US6L: First four frequencies and modes for the undamaged and damaged scenarios.

	Undamaged		Damaged (DS-US6L)		Δ (%)
	Mode	freq (Hz)	Mode	freq (Hz)	
Mode 1	1st lateral bending	8.83	1st lateral bending	8.85	0.23
Mode 2	Vertical bending	9.07	Vertical bending	9.10	0.33
Mode 3	Torsional	14.45	Torsional	14.46	0.07
Mode 4	2nd lateral bending	18.77	2nd lateral bending	18.75	−0.11

significant changes in the stress distribution. Despite the asymmetric damage, slight differences were also found in terms of maximum vertical displacement at the mid-span of the bridge (Fig. 10). Similarly, the first natural frequencies and the corresponding global modes of the structure are very slightly affected by the damage scenario, as shown by the comparison in Table 4. Of particular interest is the torsional mode, which was expected to be the most seriously affected by the asymmetry introduced in the bridge geometry by the removal of a stringer, did not change its frequency value. As for the negligible frequency increase in Table 4, the same comments made on Table 3 also apply. As a matter of fact, the global stiffness of the bridge was not affected by the failure of a stringer, revealing high robustness of the bridge structure in this type of DS.

To assess the impact of the removal of a stringer on the rail-sleeper superstructure, Fig. 11 shows the deformed configurations and the vertical displacement maps of the rail-sleeper system in the undamaged and damaged condition. From the front view a very small difference it can be noted between the left and right vertical settlements (less than 1 mm). The maximum stress in the rail superstructure was very low (less than 50 MPa also in the damaged scenario). This confirms the ability of the whole structure to appropriately compensate for the lack of a stringer element.

The negligible impact of this DS on the structure is also shown by the diagrams provided in Fig. 12-a and Fig. 12-b where the principal stress history is plotted during the train passage with reference to a point in the middle-span stringer element US6R, on the right side of the bridge, and to a point on the transversal beam UT6. Both the monitored elements were very slightly affected by this DS.

4.3. Structural response of the bridge: Secondary elements (SE)

4.3.1. Damage scenario DS-LC6L

Fig. 13 shows a comparison in terms of principal stress contour maps between the FE results obtained considering both undamaged and damaged states when the lower chord LC6L was removed from the bridge. The diagonal D6L was also removed since this element: i) was connected to the removed lower chord, ii) was unloaded due to the considered damage scenario, and iii) would not be involved in the stress transfer mechanism. In this condition, the damage completely changed the structural response of the bridge during the passage of the train. Indeed, when comparing Fig. 13-a with Fig. 13-b, it can be inferred that stress migrated from the lower to the upper part of the bridge that caused the lower bracing to experience higher tensile stresses (with increases of more than 300%, as it will be shown by the study of the stress changes in some of the most affected elements). In fact, the lower horizontal braces no longer performed only the bracing function but helped the structure to maintain its original function, characterized by a tensioned lower chord and a compressed upper chord. Given the extent of the damage, this function was compromised in any case and the upper chord showed high levels of tensile stresses caused by: i) clear torsional effects due to the different stiffness of the lateral elements, and ii) local bending effects on the upper chord. So, both elements, upper chord and lower bracing, experienced high stress increases due to the failure of lower chord LC6L.

Vertical displacement contours are provided in Fig. 14. The maximum displacement at the mid span, d_{ymax}, increased by almost 34% due to damage. The comparison between the front view (in the vertical x-y plane) of the undamaged and damaged cases shows an asymmetrical deformed bridge shape with the different involvement of the left and

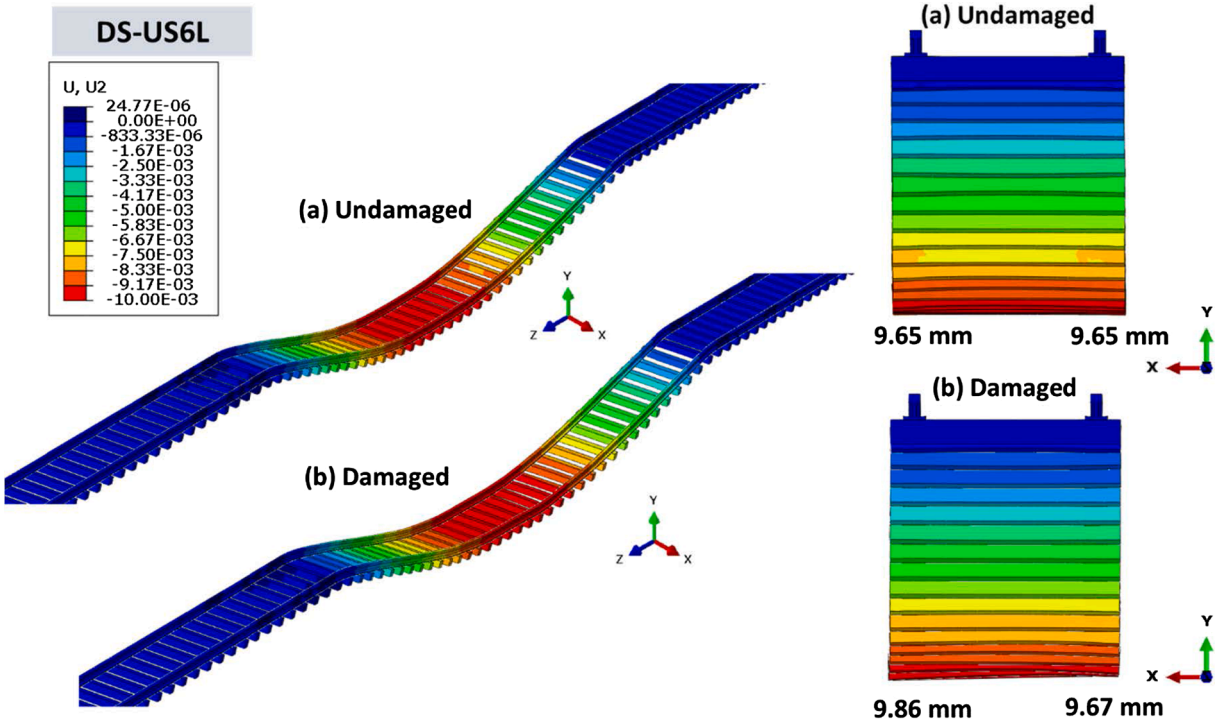

Fig. 11. DS-US6L: Displacement maps of the rail-sleepers superstructure considering both undamaged (a) and damaged (b) states. Legend units in m.

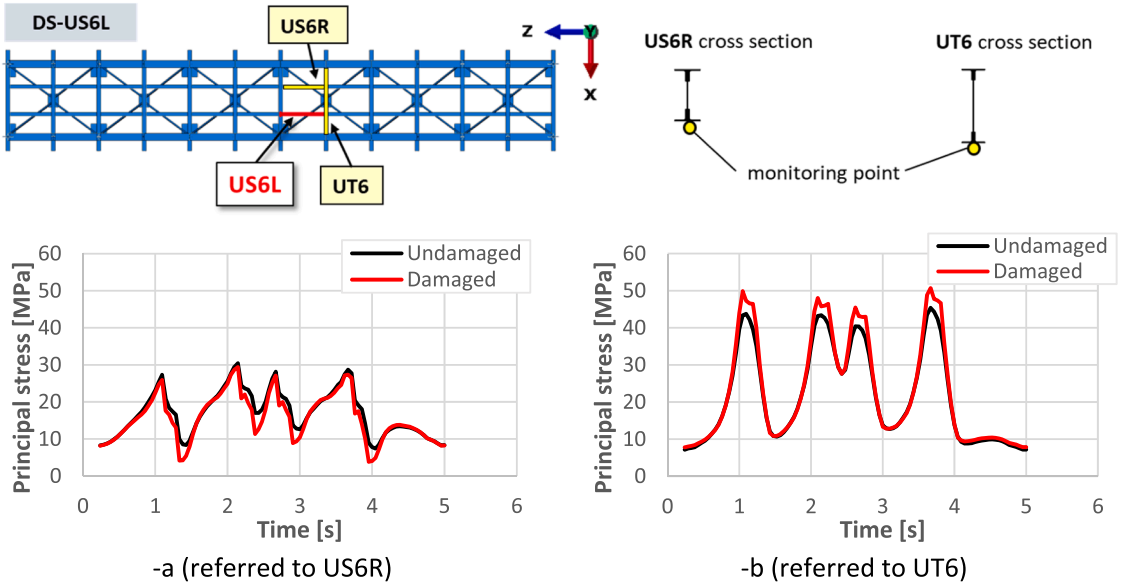

Fig. 12. DS-US6L: Principal stress histories monitored on stringer US6R (-a) and on beam UT6 (-b) considering both undamaged and damaged states.

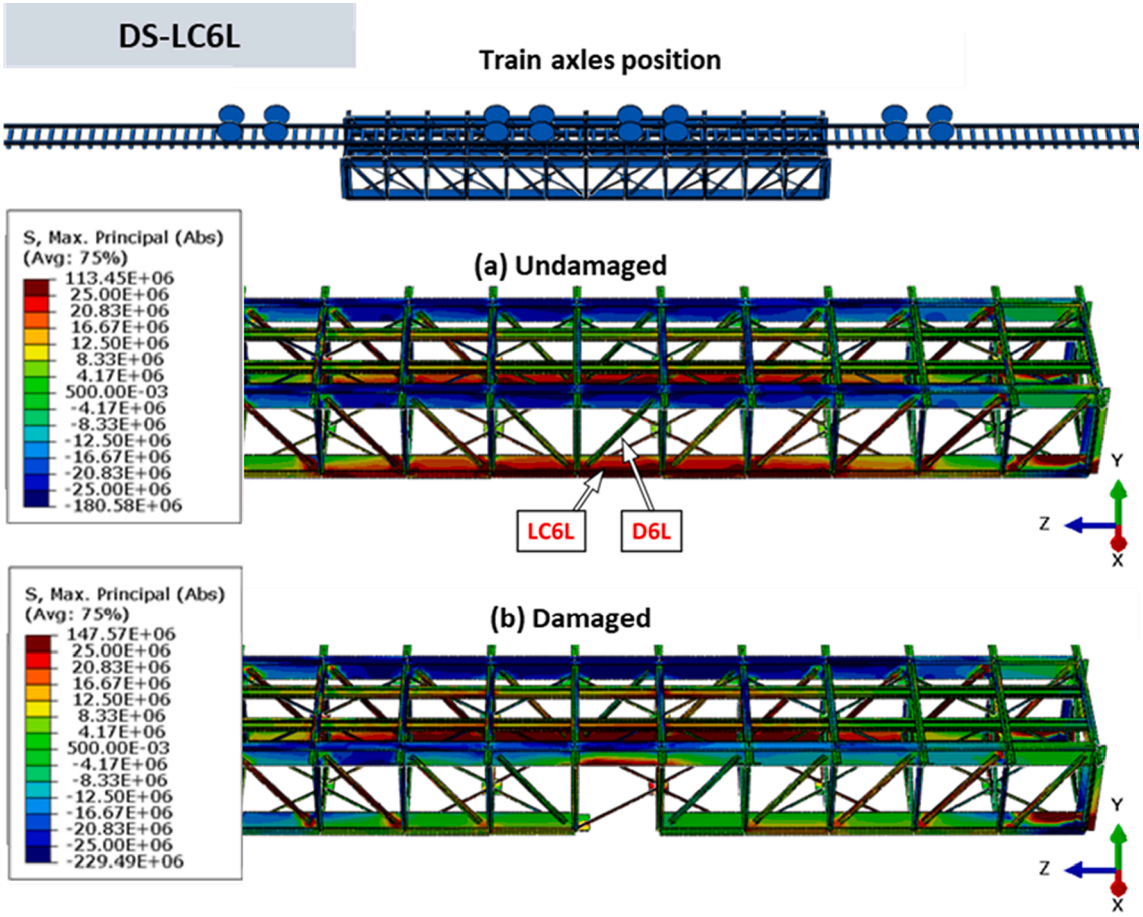

Fig. 13. DS-LC6L: Principal stress contour maps obtained considering initial undamaged (a) and damaged (b) states. Units in Pa.

right Pratt trusses, also leading to torsional effects. Of the six DSs considered in the study, this is in fact the most critical one. The removal of the lower chord markedly affected the fundamental mode of the system, leading to a frequency reduction from 8.83 Hz (undamaged scenario) to 7.20 Hz, with a decrease of more than 18 %. This first fundamental mode shape switched from lateral bending to vertical bending (see Table 5). The other modes were not significantly affected, as shown in Table 5. Despite the asymmetry this damage introduced in the original symmetric structure, the torsional mode frequency was very slightly affected.

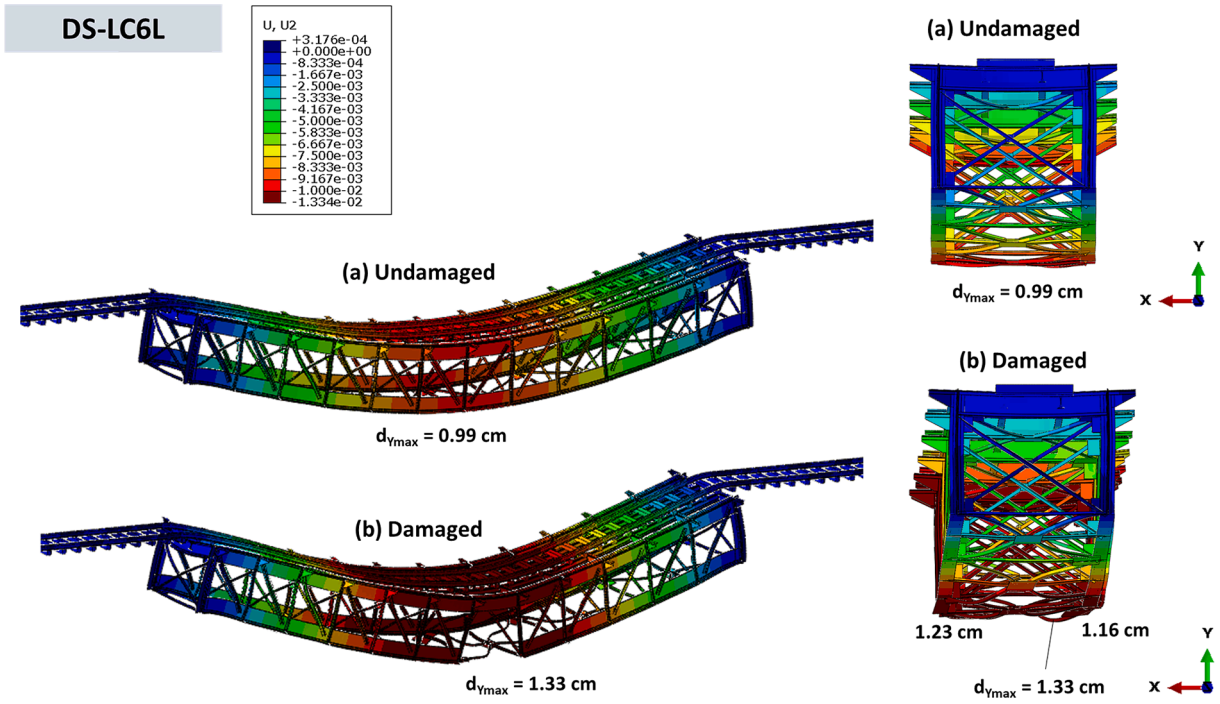

Fig. 14. DS-LC6L: Vertical displacement contour maps considering both undamaged (-a) and damaged (-b) states. Legend units in m.

Table 5
DS-LC6L: First four frequencies and modes for the undamaged and damaged scenarios.

	Undamaged		Damaged (DS-LC6L)		Δ (%)
	Mode	freq (Hz)	Mode	freq (Hz)	
Mode 1	1st lateral bending	8.83	Vertical bending	7.20	−18.46
Mode 2	Vertical bending	9.07	1st lateral bending	8.96	−1.21
Mode 3	Torsional	14.45	Torsional	14.65	1.38
Mode 4	2nd lateral bending	18.77	2nd lateral bending	18.31	−2.45

This damage scenario was investigated more in depth since it was critical. Fig. 15a contains a bar diagram comparing the Von Mises stress peaks in some of the most affected elements and shows a migration of stress from the left Pratt truss (to which the damaged elements belong) to the right one, and from the lower part of the structure to the upper. This can be inferred for instance by the reduction of stress in left-side chords (65% less in UC4L and more than three times in LC5L) and the stress increase in right-side chords (more than 50% in LC5R, UC5R and UC6R). From the bar diagram a migration of stress from the central part of the structure, where the damaged elements were, to the peripheral, can also be inferred. This is proved for instance by the 30% stress reduction in column C5L and the 25% increase in column C1L.

The FE results also show that braces and transversal beams play the role of "stress conveyors" collaborating the migration of stress from the left to the right side of the bridge. In playing this role, the lower brace LB6L increased its stress by more than three times (see Fig. 15a), while elements like the upper chord UC6L, although changing their general behaviour from compression to bending after damage, did not experience higher stress.

The time-histories of the principal stresses monitored in two of the most demanded elements, the upper chord UC6R and the lower brace LB6L, are shown in Fig. 15b and 15c. The compression stress in UC6R increased by about 50 %, while the tension stress in LB6L was up to five times higher after damage.

To check the impact of this critical DS on the rail-sleepers, the time-histories of deflection and principal stresses at the rail mid span are also plotted in Fig. 15c and Fig. 15d for the undamaged and damaged scenarios. A comparatively high increase of the maximum vertical rail deflection (more than 30%) occurred in the rail superstructure after damage, with a peak of 12.6 mm. The rail maximum stress (compressive) at the mid span went from about 21 MPa to 55 MPa, more than doubling its value, although being very much lower than the material strength.

4.3.2. *Damage scenario DS-UC6L*

Like DS-LC6L, the bridge structural response was analysed after removing the upper chord UC6L. Fig. 16 provides the principal stress contour maps relevant to the damage scenario in this section and shows a marked stress migration mainly from left (affected by damage) to right after the removal of upper chord UC6L. The vertical displacement contours displayed in Fig. 17 show a maximum increase of deflection of about 30% on the damaged side of the structure. A marked lack of symmetry can be noted in the displacement contours of the damaged structure in the X-Y vertical plane (see Fig. 17), also involving torsional effects. Although less markedly than in DS-LC6L, the frequency values decreased significantly also in this DS, as can be inferred from Table 6. The fundamental lateral bending frequency fell by about 12%, which is a comparatively significant reduction, while the torsional frequency dropped by more than 4%. On the other hand, the vertical bending and second lateral bending modes were much less affected by this damage scenario.

Fig. 18-a provides a bar diagram with the Von Mises stress peaks reached by some of the elements affected by the DS. The histogram shows a top-down stress migration from the left to the right side of the bridge, after the removal of elements on the left side. This is shown for instance by the reduced stress in elements like LC5L and UC5L and by the stress increase in others like LC6R and UC5R. Again, some elements collaborated to convey the stress from left to right and top-down, for instance brace US6L (which almost doubled its stress after damage) and the transversal beams UT6 (60% more highly loaded). The stress

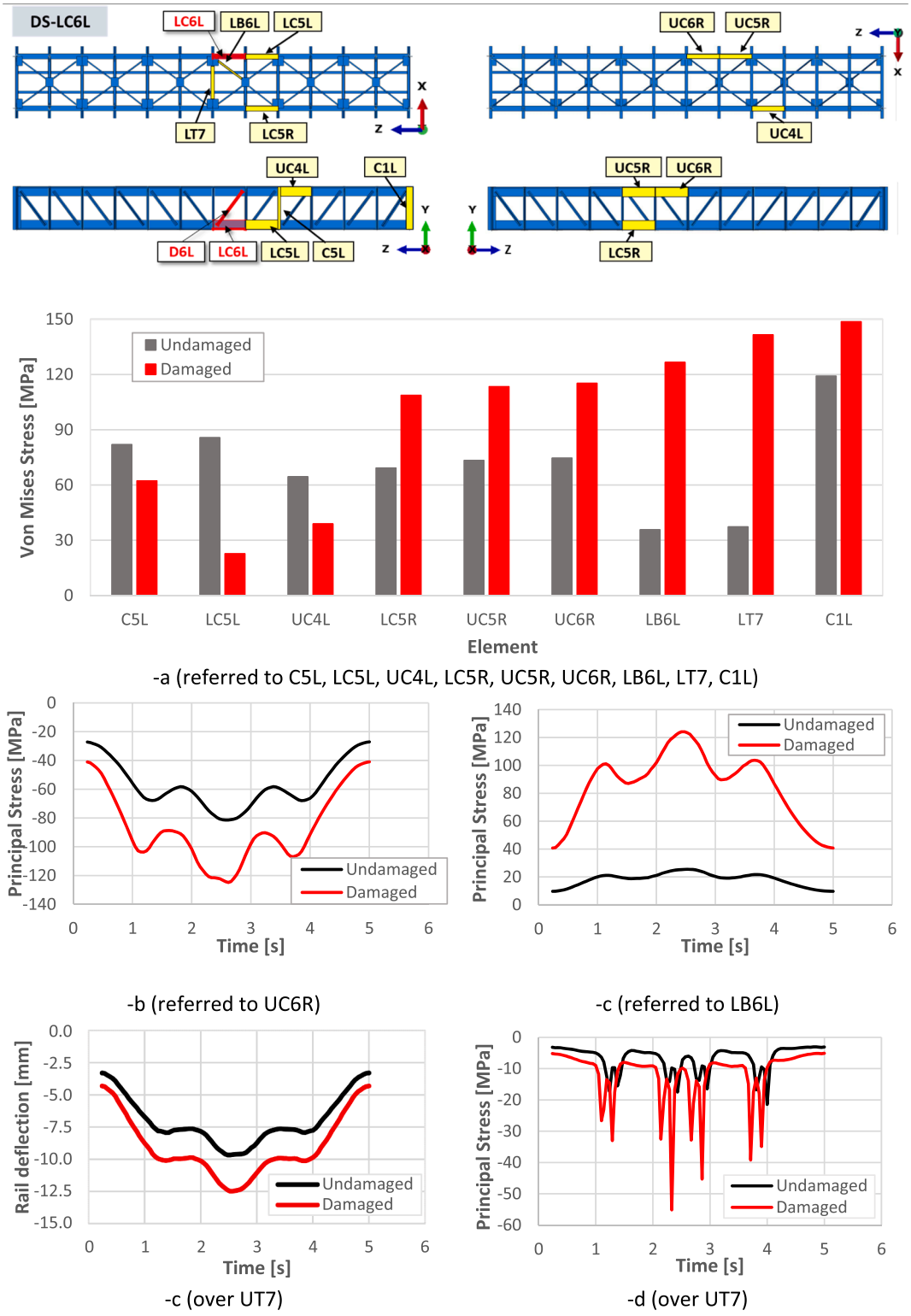

Fig. 15. DS-LC6L: (-a) Bar diagram of the Von Mises peak stresses in some of the most involved elements. Principal stress histories monitored on elements UC6R (-b) and LB6L (-c) considering both undamaged and damaged states. Vertical displacements (-c) and principal stress (-d) histories at the midspan of the rail superstructure.

migrated also from the central part of the structure to the periphery, as shown for instance by the 11% reduction in column C7L and the 20% increase in column C1L.

The principal stress histories recorded in two of the most critical elements monitored, the upper chord UC5R and the upper brace UB6L, are shown in Fig. 18b-c. The compressive stress on UC5R increased by about 30%, which may require buckling checks in other loading situations. The stress on UB6L changed from tension to compression and increased in value up to nine times after the removal of UC6L, which may represent a dangerous local condition.

The time histories of the vertical displacements and stresses of the rail at its midspan are shown in Fig. 18c and 18d. The maximum rail deflection was 12.1 mm with an increase of 25% with respect to the undamaged case. The maximum stress at the rail midspan increased

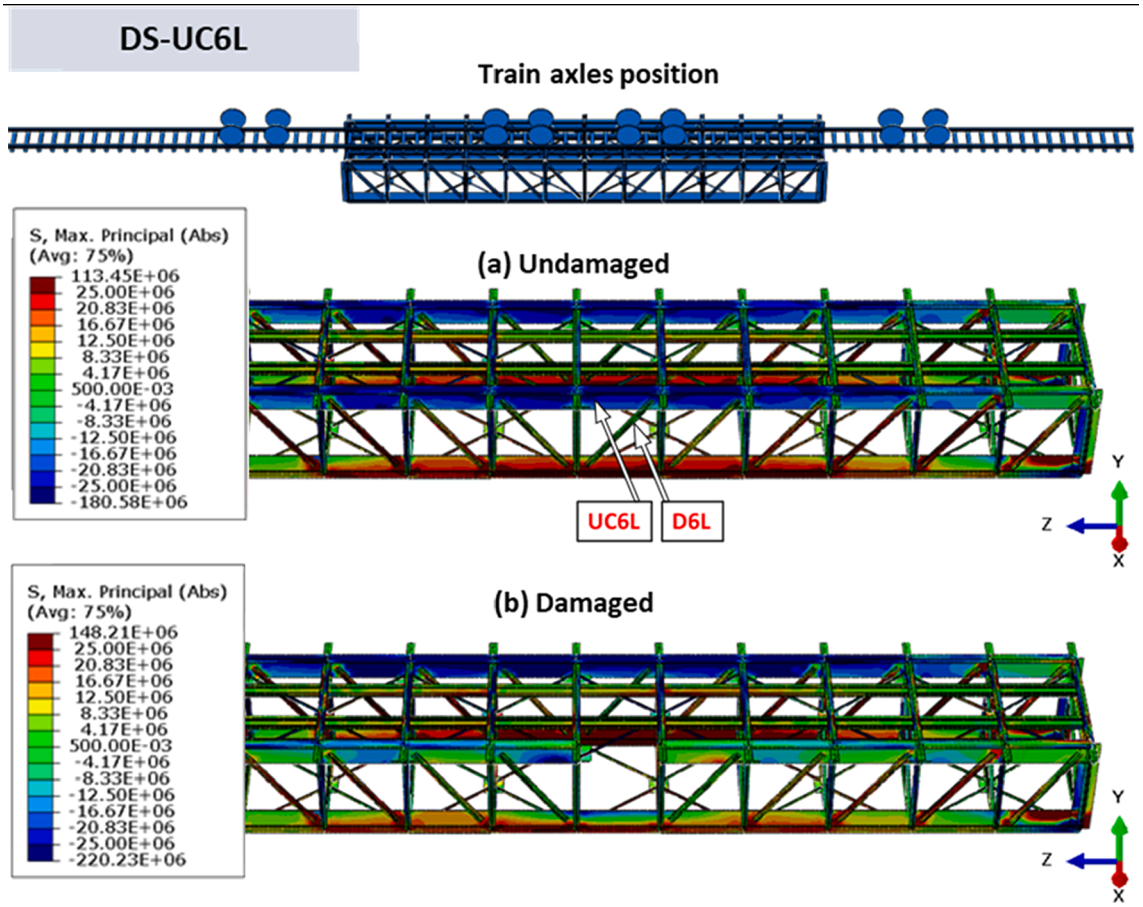

Fig. 16. DS-UC6L: Principal stress contour maps obtained considering undamaged (a) and damaged (b) states. Units in Pa.

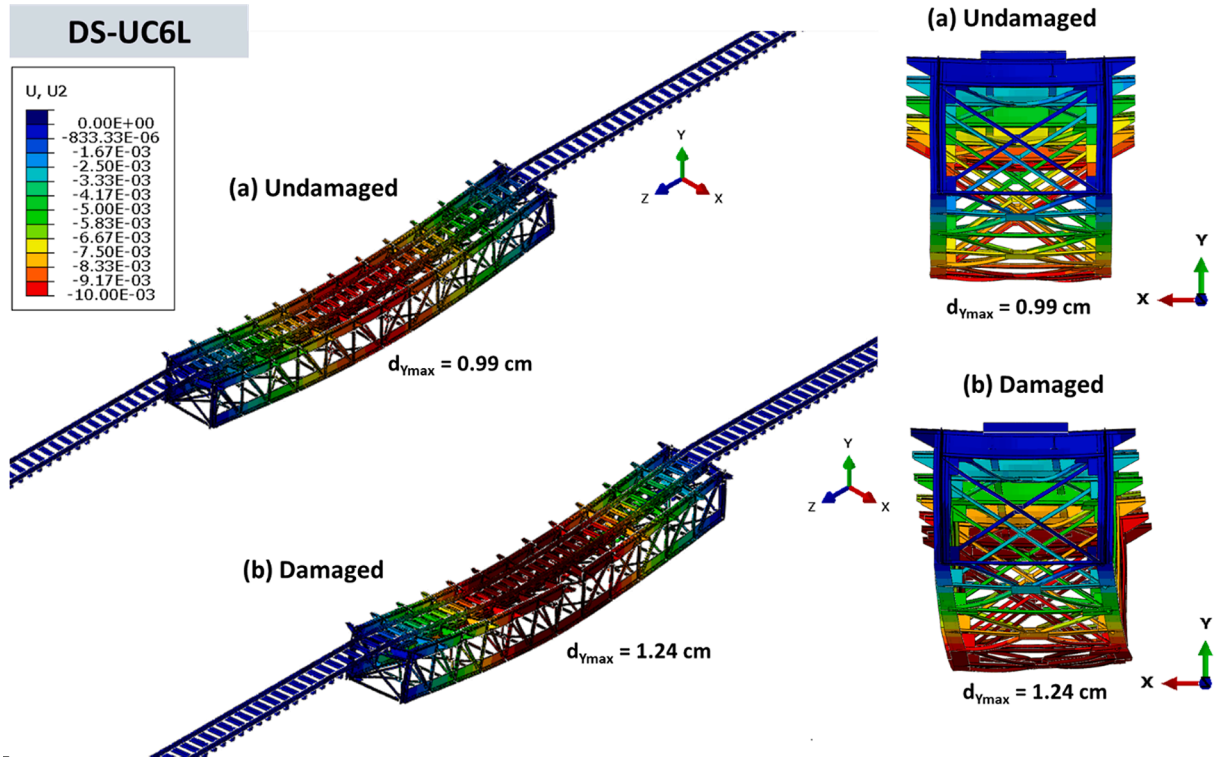

Fig. 17. DS-UC6L: Vertical displacement contour maps considering both undamaged (-a) and damaged (-b) states. Legend units in m.

Table 6
DS-UC6L: First four frequencies and modes for the undamaged and damaged scenarios.

	Undamaged		Damaged (DS-UC6L)		Δ (%)
	Mode	freq (Hz)	Mode	freq (Hz)	
Mode 1	1st lateral bending	8.83	1st lateral bending	7.90	−10.53
Mode 2	1st vertical bending	9.07	1st vertical bending	8.99	−0.88
Mode 3	1st torsional	14.45	1st torsional	13.87	−4.01
Mode 4	2nd lateral bending	18.77	2nd lateral bending	18.42	−1.86

instead by about 63%. This DS was found to be very demanding on both the bridge structure and the rail, although less critical than the scenario in which the lower chord failed (DS-LC6L). This occurred since the upper horizontal structure is more robust (bracings, beams and stringers) than the lower (bracings only) and more efficiently able to transfer the load from left to right.

4.3.3. Damage scenario DS-D3L

Fig. 19 gives a close-up view of the principal stress contours relevant to the failure of diagonal D3L, in accordance with previous damage scenarios in a time-step in which the train is at the centre of the bridge. From a comparison of the stress contours, a relatively limited effect can be noted in terms of activation of alternative load paths in the considered damage scenario. Locally, the removing the diagonal increased the stress level on the adjoining lower and upper chords, while the overall structure response was slightly altered by the DS. This is also confirmed by the maximum vertical displacement found after the element removal, which showed a moderately increased deflection on the bridge's damaged side (Fig. 20). Accordingly, the DS frequencies slightly changed with respect to the undamaged case (see Table 7).

The limited impact of this scenario on the overall behaviour of the structure can also be inferred from the bar diagram provided in Fig. 21-a, where the peaks of the Von Mises stresses in some affected elements are displayed with reference to the undamaged and damaged cases. A group of elements (C3L, D2L, UC3L, LC3L, LB3L) around the affected diagonal are firstly considered in the diagram, then reference to a second group of more distant elements (UT3, D2R, LC3R, C2L) is also made. It can be noted that the first group experienced a moderate stress increase or decrease, while the second group was almost unaffected by the DS. This shows a local redistribution of the stress after damage, the bridge structure being only slightly affected by the removal of the diagonal.

Two monitoring points were chosen to analyse the evolution of the stress demand, one on diagonal D2L (see Fig. 21-a) and the other one on lower chord UC3L (see Fig. 21-b). The principal stress histories in Fig. 21-a and Fig. 21-b show that the removal of diagonal D3L led to a small increase of tensile stress in diagonal D2L (about 17%) and of compressive stress in chord UC3L (35%).

The rail was almost unaffected by this DS: the maximum stress increased by only 15 % (the final Von Mises peak value being 37.5 MPa), while the peak midspan deflection went from 9.7 mm to 10.0 mm.

4.3.4. Damage scenario DS-C2L

Fig. 22 gives the results of DS-C2L, where the damage comprised the removal of column C2. A comparison between the principal stress contour maps provided in Fig. 22-a and -b shows an increase of the compression stresses on the upper and lower chords near the removed column. In fact, the shear transmission along the Pratt-truss is interrupted when column C2L is removed, causing higher bending stresses on the upper and lower chords.

The vertical displacement contour maps provided in Fig. 23 show a very low vertical displacement increase in the damaged structure and a moderate reduction of the main frequency values (less than 3%) (see Table 8).

To assess the propagation of stress after damage, Fig. 24 provides a bar diagram with the peaks of the Von Mises stresses reached in some elements before and after the removal of the C2L column. The first group considered in the diagram collects elements (C1L, D2L, D1L, UC2L, LC2L) that lie on the left-side Pratt truss and are close to the damaged column, while the second group of elements (UC2R, D1R, LC1R, C1R) belongs to the right-side Pratt truss. The results show that the DS affected only the elements in the vicinity of the damaged column, the stress increase in the latter being generally lower than 60%.

Fig. 24b-c provides the stress histories of a passing train for the undamaged and damaged conditions at two of the most seriously affected elements: diagonal D1L and upper chord UC2L. Both the compressive stress in diagonal D1L and the tension stress in UC2L increased by about 50 % when C2L failed. The rail was slightly affected in this DS: i.e., only a 3 % increase in vertical deflection while the stress in the most heavily loaded point in the rail went from about 32 MPa to 48 MPa.

5. Discussion and recommendations

This section analyses in depth the previously obtained results. First an evaluation of the robustness of the bridge structure is given and valid conclusions applicable to other similar bridges are drawn. Identification and analysis of the ALPs activated after the various DSs are then performed with special attention to the ways in which they were made effective. Finally, a series of recommendations for structural bridge design and SHM based on the results are given.

5.1. Robustness assessment

Structural robustness is defined as the insensitivity of a structure to further damage after a local failure. A robust structure may also be resilient if it can adapt to local changes to restrict the spreading of the local failure to the rest of the structure. Several methods and indexes have been developed to quantify structural robustness. The evaluation of the structural robustness can be categorized into three main methodologies: deterministic, probabilistic and risk-based.

According to the deterministic evaluation, robustness can be evaluated as the ratio between the maximum displacement of the undamaged structure and the corresponding displacement in the damaged one [8,26], or as the ratio between the determinant of the stiffness matrix of the system in which an element has been removed and that of the intact system, or even as the ratio between (1-p) and p_lim where p is the maximum spread of damage and p_lim is the acceptable damage [29].

For a probabilistic evaluation, the following ratio may be adopted [30], where P_f is the probability of failure for the damaged and intact structure.

$$\frac{P\_f(damaged) - P\_f(intact)}{P\_f(intact)} \tag{1}$$

When a risk-based evaluation of structural robustness is adopted, a general expression might be adopted [26,31].

$$R = \sum_{D,H} P(C|D)\hat{A}\cdot P(D|H)\hat{A}\cdot P(H)\hat{A}\cdot Cost(C) \tag{2}$$

where R is the total risk of the structure, P(C|D) is the conditional probability of collapse C of the structure as a result of local damage D, P(D|H) is the conditional probability of local damage given event H, P(H) is the probability of occurrence of an abnormal hazard event, and Cost (C) is the cost of collapse.

In this study, a deterministic approach has been adopted, in which robustness can be quantified as [26]:

$$\rho = \frac{s_0}{s_d} \tag{3}$$

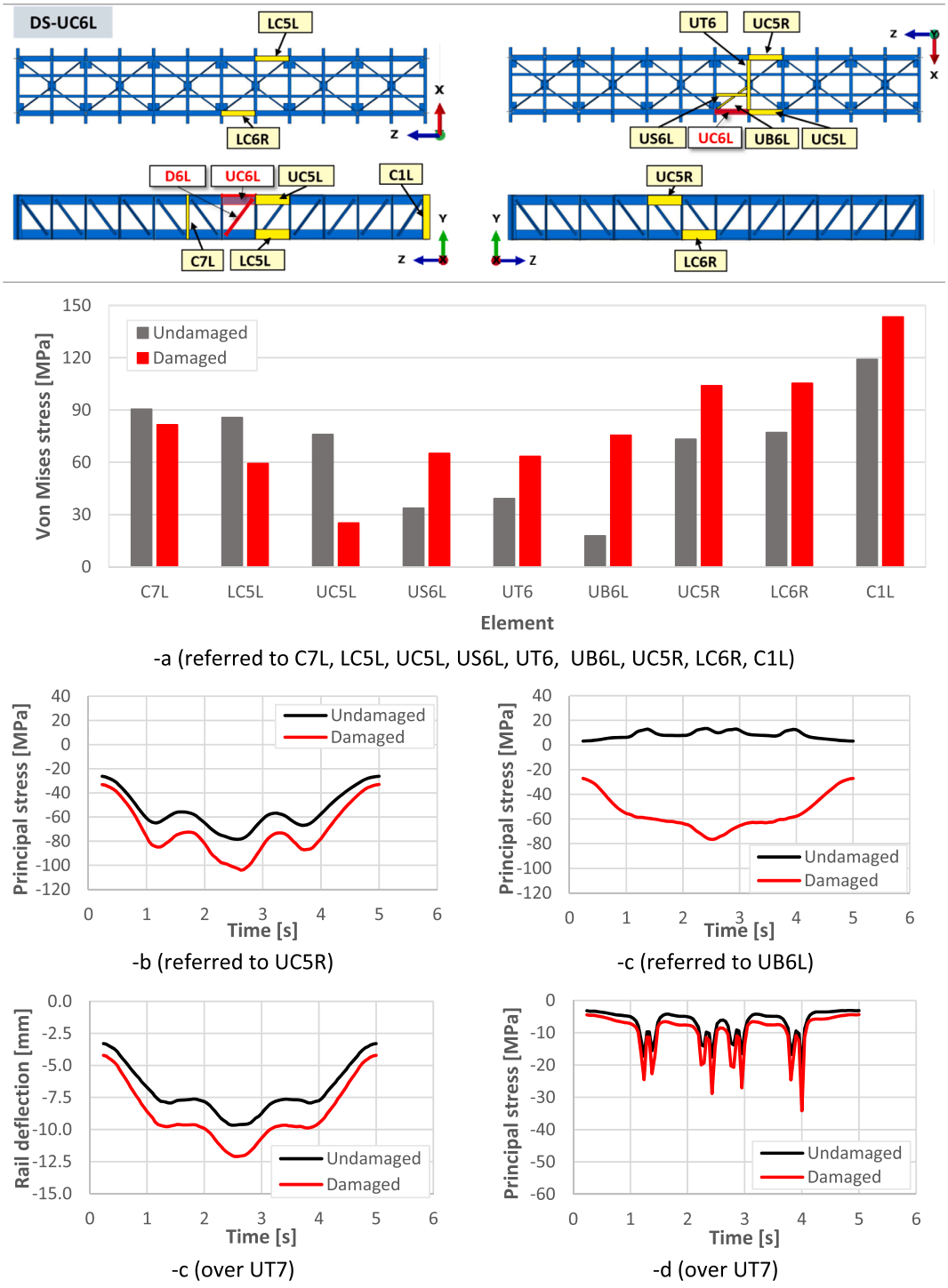

Fig. 18. DS-UC6L: (-a) Bar diagram of the maximum Von Mises stresses in some of the most critical elements, considering both initial and damaged states. Principal stress histories monitored on the upper chord UC5R (-b) and on the upper bracing UB6L (-c) in the undamaged and damaged scenarios. Vertical displacements (-c) and principal stress (-d) histories at the midspan of the rail superstructure.

Here ρ is the robustness index, while s_0 and s_d are the maximum displacements of the intact and of the damaged structure respectively.

Table 9 provides the values of the robustness index ρ for the truss—bridge structure under study, calculated for the different DSs. It is worth noting that $\rho = 1$ means that the global structure is totally insensitive to the DS while $\rho = 0$ indicates that the progressive collapse of the structure cannot be arrested. As it can be seen from the results, the considered pratt-truss structure is robust enough to withstand all the DSs without involving progressive collapse. The global response is insensitive to DS-UT7 and DS-US6L, and almost insensitive to DS-D3L and DS-C2L. As expected, the most aggressive DSs are those involving the sudden removal of a main chord, but even in these cases the robustness index is high enough (0.80 for DS-UC6L and 0.74 for DS-LC6L) to consider the main structure robust enough also against these critical DSs.

So, even though the structural response significantly changed after suffering damage in the most demanding DSs, the structure was able to avoid a full-scale collapse. This is true under the considered loading

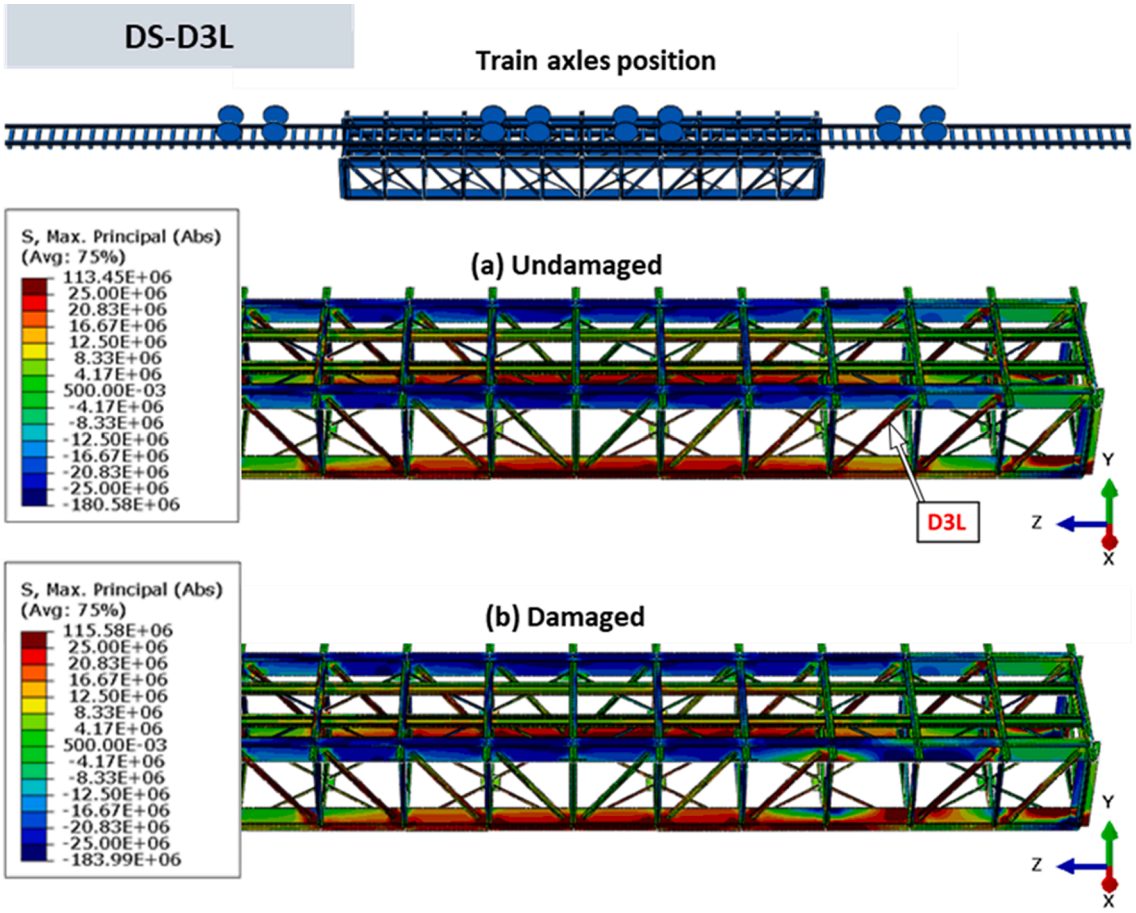

Fig. 19. DS-D3L: Principal stress contour maps obtained considering initial undamaged (a) and damaged (b) states. Units in Pa.

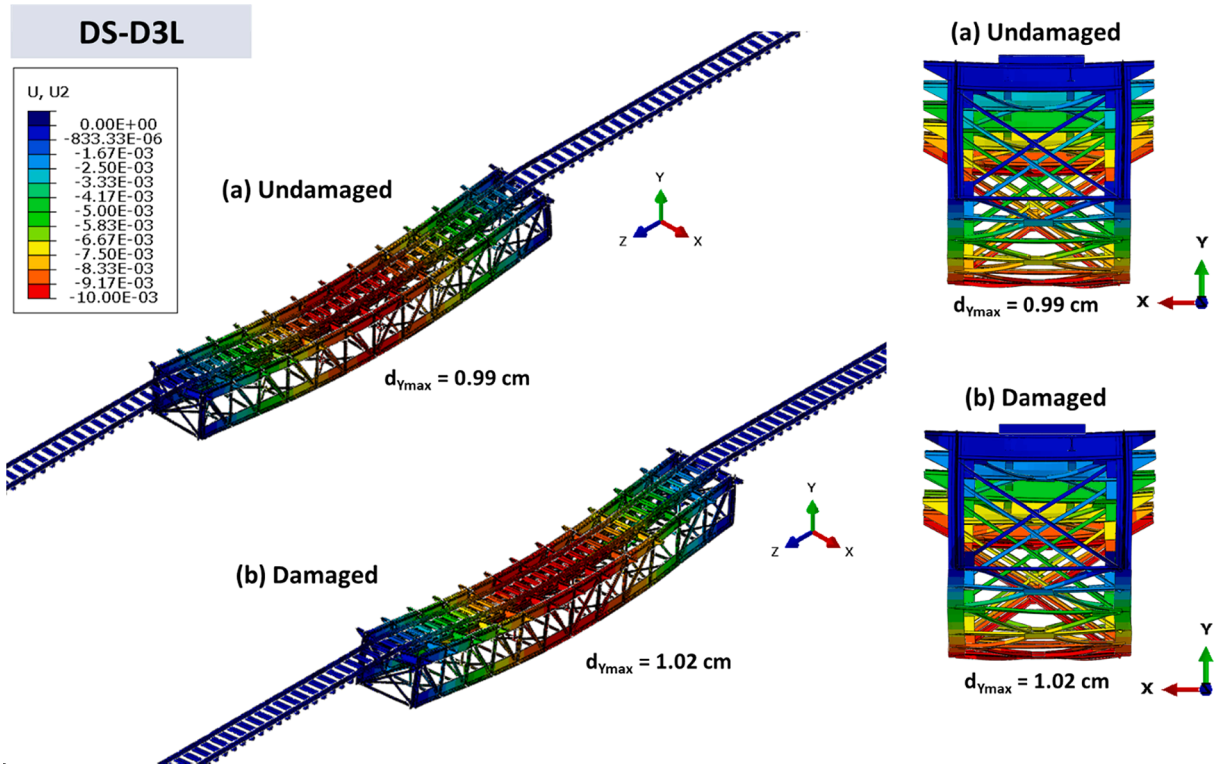

Fig. 20. DS-D3L: Vertical displacement contour maps considering both undamaged (-a) and damaged (-b) states. Legend units in m.

Table 7
DS-D3L: First four frequencies and modes for the undamaged and damaged scenarios.

	Undamaged		Damaged (DS-D3L)		Δ (%)
	Mode	freq (Hz)	Mode	freq (Hz)	
Mode 1	1st lateral bending	8.83	1st lateral bending	8.78	−0.57
Mode 2	Vertical bending	9.07	Vertical bending	8.94	−1.43
Mode 3	Torsional	14.45	Torsional	14.24	−1.45
Mode 4	2nd lateral bending	18.77	2nd lateral bending	18.80	0.16

conditions of the bridge in service. In these conditions the bridge can be said to be sufficiently robust to bear the passing of light-weight trains. However, the fact of being robust does not imply that the operating conditions of the trains passing over it are safe. Obviously, all train operations should be immediately stopped if a local failure of the type analysed here is identified. However, the local failure could have been due to a train passing over the bridge when the failure occurred. In these circumstances it is important to determine whether the train could stand the deformation caused by each damage scenario at a local level (on rails). In the DSs involving primary elements, rail vertical displacements of up to 1.5 mm were recorded over a length of 3.5 m. In the case of DSs involving secondary elements the deflections were up to 2.8 mm over a complete span of 21 m. In the DSs where primary elements failed the maximum additional slope in the rails was 0.85 mm/m while in DSs relevant to secondary elements it was 0.27 mm/m. These values are slightly above the maximums recommended by railway authorities for new interventions [32,33], so that the structure can also be considered apt for the possible transit of a hypothetical train that could cause a local structural failure in both primary and secondary elements.

The above conclusions may not be valid for heavier train traffic (e.g. conventional or high-speed trains) or other structures. It is generally known that any structure has an extra strength capacity when working under real loading conditions (due to safety factors and idealised design loads). As far as the considered steel truss-type bridge is concerned, this extra capacity should be in agreement with the increases in percentage found in the present study to consider that this structure is robust enough. The extracted results generally showed stress increases up to 65%, which should be covered by the extra strength capacity of the

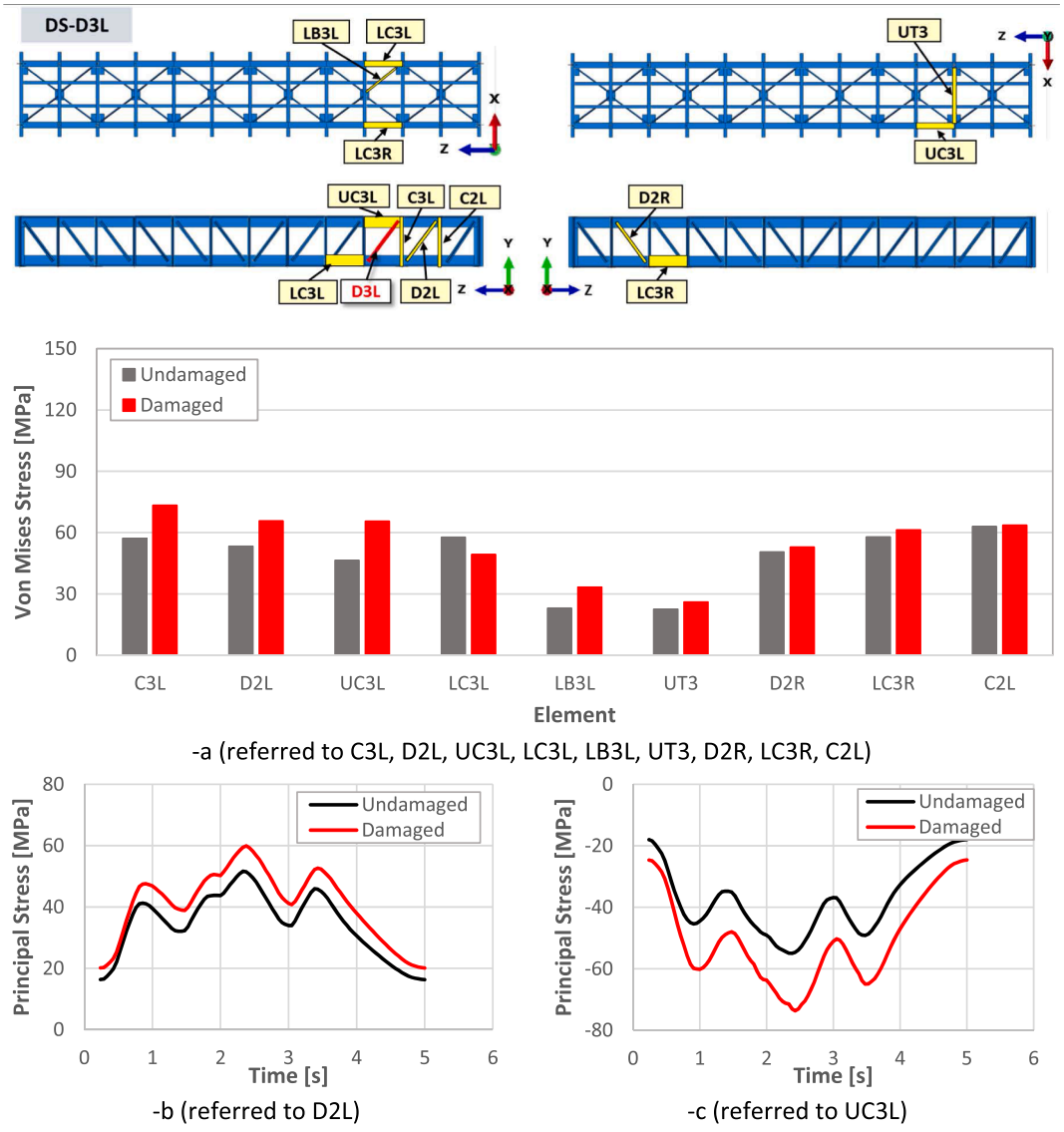

Fig. 21. DS-D3L: (-a) Maximum Von Mises stresses in some of the most affected elements considering both undamaged and damaged states. Principal stress histories monitored on the diagonal D2L (-b) and on the upper chord UC3L (-c) in the undamaged and damaged scenarios.

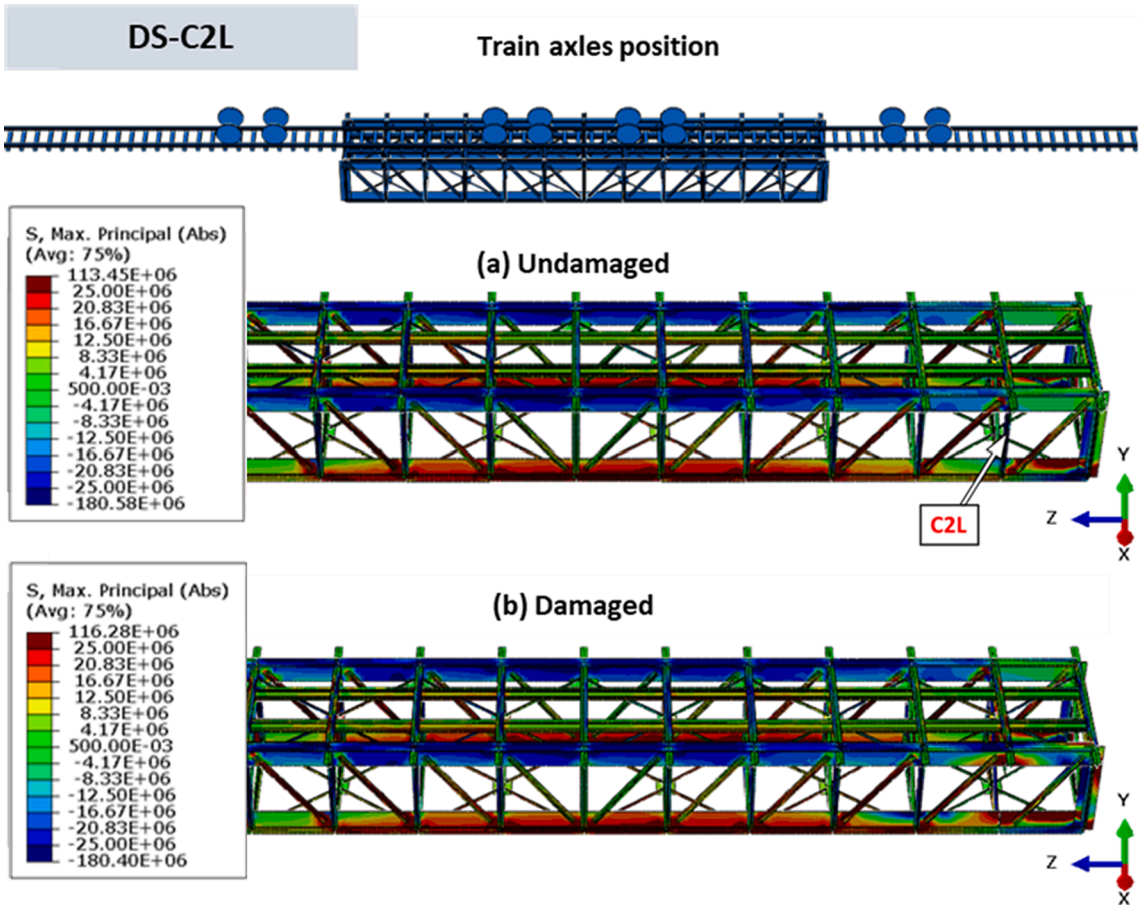

Fig. 22. DS-C2L: Principal stress contour maps obtained considering undamaged (a) and damaged (b) states. Units in Pa.

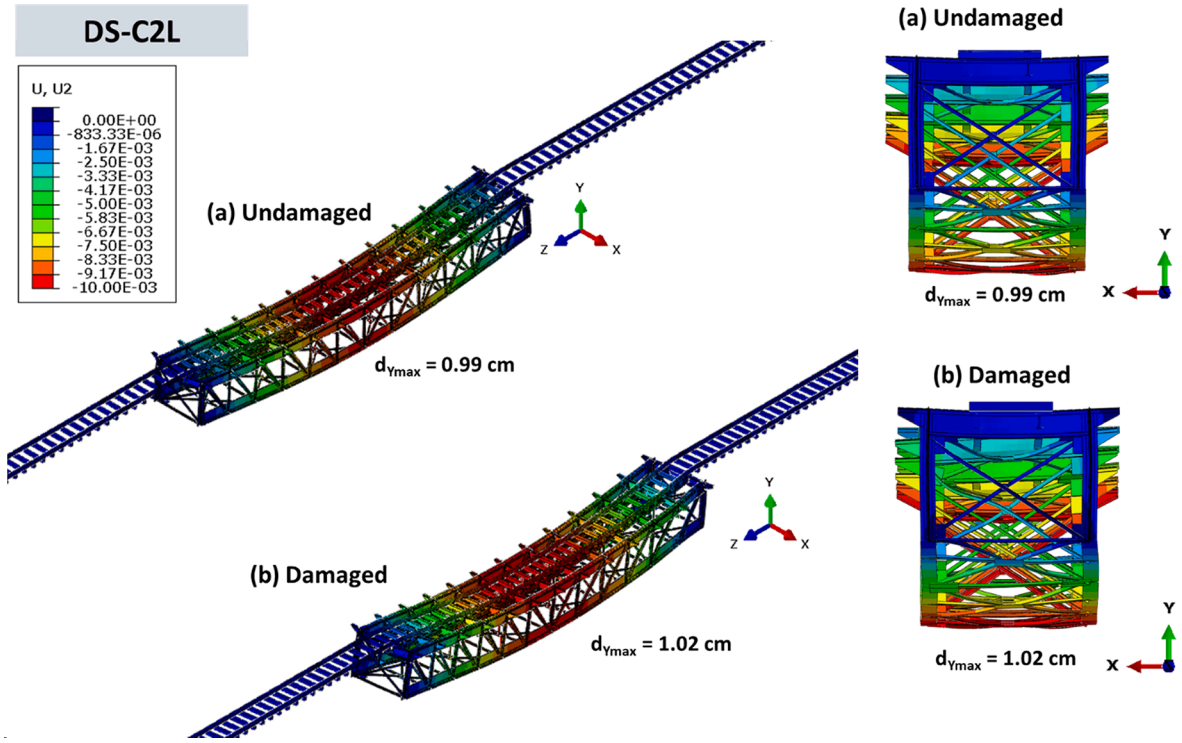

Fig. 23. DS-C2L: Vertical displacement contour maps considering both undamaged (-a) and damaged (-b) states. Legend units in m.

Table 8
DS-C2L: First four frequencies and modes for the undamaged and damaged scenarios.

	Undamaged		Damaged (DS-UC6L)		Δ (%)
	Mode	freq (Hz)	Mode	freq (Hz)	
Mode 1	1st lateral bending	8.83	1st lateral bending	8.69	−1.59
Mode 2	Vertical bending	9.07	Vertical bending	8.90	−1.87
Mode 3	Torsional	14.45	Torsional	14.07	−2.63
Mode 4	2nd lateral bending	18.77	2nd lateral bending	18.67	−0.53

considered bridge. However, some DS cases (LC6L and UC6L) showed stress increases in some elements up to nine times the original stress in the undamaged structure, which cannot be compensated by the extra strength capacity provided by the safety factors typically adopted in the design of such kind of structures.

5.2. Alternative load paths (ALPs) to the damage scenarios

Any structure is robust if it can efficiently activate ALPs after a local failure without compromising its safety. In the case dealt with in this study, the ALPs were activated within the structure's capacity in all the DSs, and the structure was found to be able to adapt to the new conditions. However, there were significant differences between the considered scenarios and different activated ALPs. Table 10 gives a summary of

Table 9
Robustness quantification of the structure for the different DSs.

	DSs	Failure description	s_0 [cm]	s_d [cm]	ρ
Primary Elements	DS-UT7	Transversal beam	0.99	0.99	1.00
	DS-US6L	Stringer or longitudinal beam	0.99	0.99	1.00
Secondary Elements	DS-LC6L	Lower Chord	0.99	1.33	0.74
	DS-UC6L	Upper Chord	0.99	1.24	0.80
	DS-D3L	Diagonal	0.99	1.02	0.97
	DS-C2L	Column	0.99	1.02	0.97

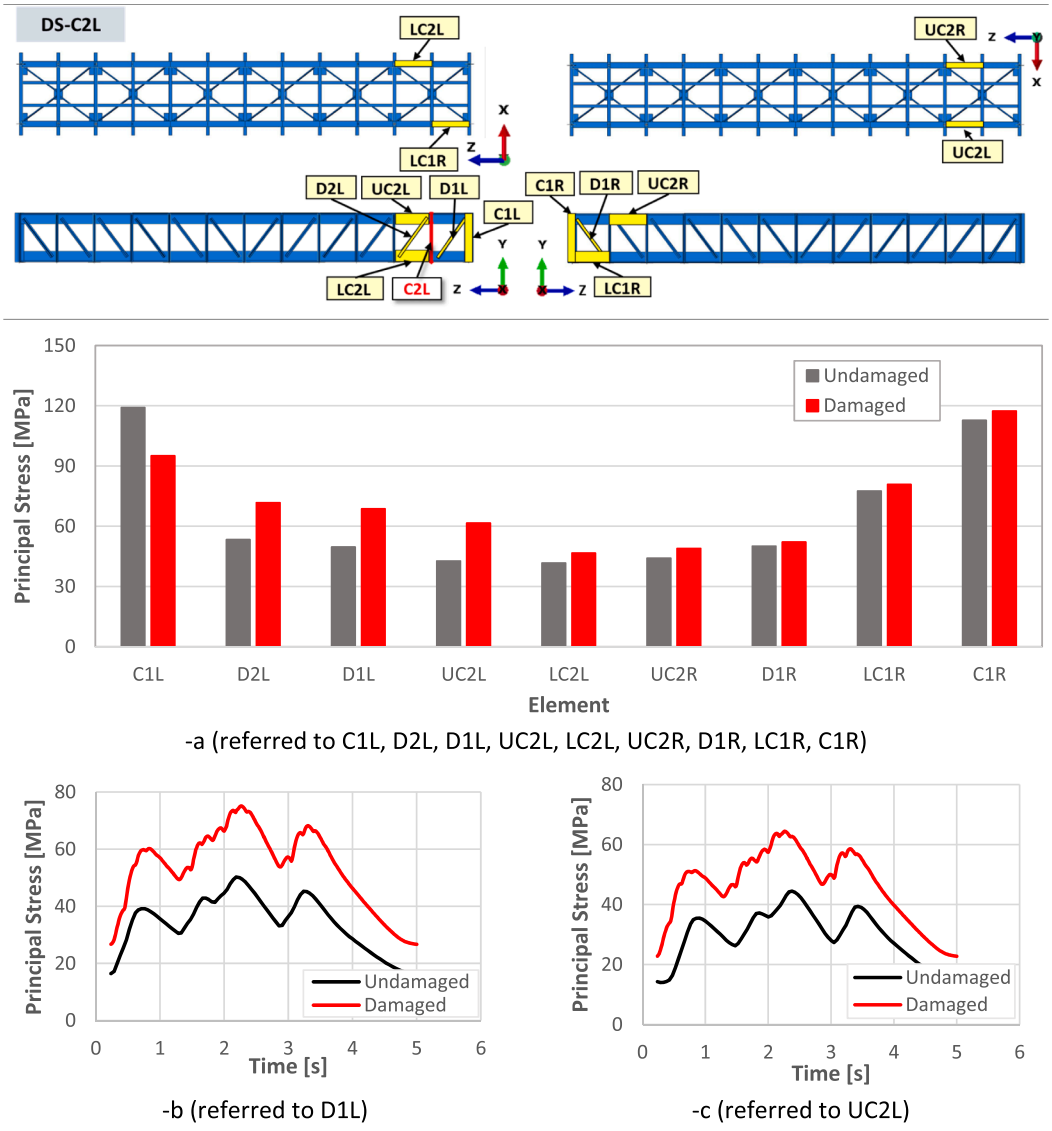

Fig. 24. DS-C2L: (a) Maximum Von Mises stresses in some of the most affected elements considering both undamaged and damaged states. Principal stress histories monitored on the diagonal D1L (-b) and on the upper chord UC2L (-c) in the undamaged and damaged scenarios.

Table 10
Main active ALPs after each DS.

	DS	Failure description	Alternative Load Paths
Primary Elements	DS-UT7	Transversal beam	Stringers working with a double span; slight contribution of rails
	DS-US6L	Stringer or longitudinal beam	Contribution of rails
Secondary Elements	DS-LC6L	Lower Chord	(i) Bending of the upper chord
			(ii) Load transmission to the other Pratt truss
	DS-UC6L	Upper Chord	Load transmission to the other Pratt truss
	DS-D3L	Diagonal	Bending of joints in a Vierendeel system
	DS-C2L	Column	Bending of joints

the main efficiently activated ALPs in the various DSs.

Regarding the DSs in primary elements, and specially in DS -UT7, the failure of a transversal beam produced a notable change in the ways the loads were transmitted and required the stringers (also the rails to some extent) to support greater loads, with a span twice the length of the original span. DS-US6L was even more critical and required the contribution of the rails working under bending stresses as the last line of defence to redistribute the local loads towards secondary elements.

Among the DSs with secondary elements, DS-LC6L simultaneously activated two principal ALPs: i) the failure of the lower chord made the upper chord to change its behaviour, mainly from compression stresses to bending stresses; and ii) the failure of the lower chord on the left side caused a load transmission to the right side raising the stress levels of the elements through which it passed (e.g. lower horizontal bracing) and the Pratt-truss elements on the right. This, however, did not happen in DS-UC6L, where the main ALP was only the load transmitted to the right. In this last case (DS-UC6L) the elements that allowed the load to be transmitted from the left to the right side (i.e. transversal beam and stringers, upper horizontal bracing) were much more resistant than in DS-LC6L (with only lower horizontal bracing) and caused: i) this to be the predominant ALP, and ii) the lower chord did not have to bear considerable bending stresses.

In DS-D3L the failure of a diagonal clearly changed the local structural configuration of this zone from that of a Pratt truss to a Vierendeel beam, thus requiring higher resistance to bending stresses at the joints. This situation with bending stresses is not common with Pratt trusses, in which the structure can find its equilibrium with only axial stresses and residual bending stresses.

Finally, in DS-C2L the failure of one column required the joints in the upper and lower chords to be able to absorb bending stresses.

5.3. Recommendations

This section gives a series of practical recommendations deduced from the results obtained in the study and the discussion done up to this point.

When designing new structures like the one here studied, it is recommended to do a preliminary analysis like the one carried out in the present paper in order to design robust bridge elements able to activate efficient ALPs in case of a local failure. Alternatively, some key elements can be over-designed (e.g. bracing elements and main chords) and a good connection between the superstructure (i.e. sleepers and rails) and the structure should be ensured. Structural continuity is also especially important in the nodes to give the structure sufficient ability to absorb bending stresses at the joints. This last recommendation is not common when designing Pratt trusses but should be addressed if the aim is to achieve a robust structure.

For existing steel truss-type bridges two approaches are recommended: i) reinforce the structures to comply with the robust criteria referred to above, and/or ii) monitor critical elements in real time, especially in cases that do not comply with the robust criteria, to anticipate the complete failure of a local element that could cause a progressive collapse. This last option can be carried out by means of strain, displacement and acceleration sensors. The strain sensors should be placed at points in the cross section at which increased strain is higher after, or during, the failure of an element. As it could be seen from the analysis and the results obtained, the elements generally suffer significant increases in both axial and bending stresses. Early detection of the failure of an element will be simpler if the strain sensors are placed far away from the centre of gravity of the cross section. A complete series of recommendations for strain, displacement and acceleration sensors can be found in Buitrago et al. [16].

Throughout the study, the acceleration sensors and FFTs showed that the fundamental frequencies of the damaged structure were significantly reduced only in the case of serious damage. The most sensitive of these frequencies is associated with the 1st lateral bending and so it is the fundamental frequency that should be controlled. However, it is quite difficult to anticipate any local failure by means of monitoring the fundamental frequencies. In fact, vibration-based methods of structural damage detection are typically based on monitoring changes of more sensitive parameters than the frequency such as the mode-shape curvature or the curvature of the Frequency Response Function [34].

The knowledge and recommendations extracted in this study are being applied to three real truss-type bridges in the region of Valencia (Spain) with more than 400 strain, temperature, displacement and acceleration sensors in a real-time monitoring system with a series of automatically checked alarms. Further results, conclusions and recommendations are expected to be extracted from this acquired experience and the big-data analysis in the coming years.

6. Conclusions

This paper describes a complete evaluation of the robustness of steel truss-type bridge structures based on the case study of an actual bridge, the results of which were used to draw conclusions and make recommendations. The study of robustness consisted of computer simulations of different Damage Scenarios (DSs) to examine the structure's capacity to activate Alternative Load Paths (ALPs). The scenarios included a series of non-simultaneous failures of different elements that together represented the behaviour of the entire structure: a transversal beam and a longitudinal beam (stringer) of the primary system, a lower and an upper chord, a diagonal and a column of the secondary system. After the analysis of the results the bridge's robustness was assessed together with an analysis of the significant and efficient ALPs activated, after which some recommendations were made. The study's conclusions were as follows:

- In the different DSs the structure was able to avoid the repercussions of the local failure in the form of a progressive collapse. This conclusion may not be valid for other types of train or other types of structures, which would require a more in-depth analysis.
- After each of the local failures efficient ALPs were activated that required the structural contributions of: i) elements with higher stresses than those generated in the undamaged structure, ii) elements working with a different structural configuration, (iii) elements of the superstructure such as rails, and (iv) joints under bending stresses.
- It is recommended that new or existing truss-type bridge structures be designed or retrofitted following the methodology used in the study. Alternatively, key structural elements should be over-designed, to allow the efficient activation of ALPs; joints should be given with higher resistance to bending stresses; and the structure and superstructure should have a strong connection to allow load transfer between them.

- Continuous structural monitoring is also recommended with the optimal arrangement of sensors to be able to predict in time the occurrence of local failures and prevent the complete failure of the entire structure.

CRediT authorship contribution statement

Giacomo Caredda: Data curation, Software, Investigation. **M. Cristina Porcu:** Methodology, Investigation, Data curation. **Manuel Buitrago:** Conceptualization, Methodology, Investigation. **Elisa Bertolesi:** Investigation, Validation. **José M. Adam:** Conceptualization, Investigation, Supervision.

Declaration of Competing Interest

The authors declare that they have no known competing financial interests or personal relationships that could have appeared to influence the work reported in this paper.

Acknowledgements

We would like to express our gratitude to the FGV agency (Ferrocarrils de la Generalitat Valenciana), Calsens company and Juan Antonio García Cerezo, of FGV, for their invaluable cooperation and recommendations. This article has received funding for open access charge: CRUE-Universitat Politècnica de València.

References

[1] Deng L, Wang W, Yu Y. State-of-the-Art Review on the Causes and Mechanisms of Bridge Collapse. J Perform Constr Facil 2016;30:04015005. https://doi.org/10.1061/(ASCE)CF.1943-5509.0000731.
[2] Biezma MV, Schanack F. Collapse of Steel Bridges. J Perform Constr Facil 2007;21:398–405. https://doi.org/10.1061/(asce)0887-3828(2007)21:5(398).
[3] National Transportation Safety Board. Collapse of the I-5 Skagit River Bridge Following a Strike by an Oversize Combination Vehicle in Mount Vernon, Washington May 23, 2013. Washington D.C.: 2014.
[4] Birajdar HS, Maiti PR, Singh PK. Failure of Chauras bridge. Eng Fail Anal 2014;45:339–46. https://doi.org/10.1016/j.engfailanal.2014.06.015.
[5] Wardhana K, Hadipriono FC. Analysis of Recent Bridge Failures in the United States. J Perform Constr Facil 2003;17:144–50. https://doi.org/10.1061/(asce)0887-3828(2003)17:3(151).
[6] Brunesi E, Nascimbene R, Parisi F, Augenti N. Progressive collapse fragility of reinforced concrete framed structures through incremental dynamic analysis. Eng Struct 2015;104:65–79. https://doi.org/10.1016/j.engstruct.2015.09.024.
[7] Fascetti A, Kunnath SK, Nisticò N. Robustness evaluation of RC frame buildings to progressive collapse. Eng Struct 2015;86:242–9. https://doi.org/10.1016/j.engstruct.2015.01.008.
[8] Adam JM, Parisi F, Sagaseta J, Lu X. Research and practice on progressive collapse and robustness of building structures in the 21st century. Eng Struct 2018;173:122–49. https://doi.org/10.1016/j.engstruct.2018.06.082.
[9] Adam JM, Buitrago M, Bertolesi E, Sagaseta J, Moragues JJ. Dynamic performance of a real-scale reinforced concrete building test under corner-column failure scenario. Eng Struct 2020;210:110414. https://doi.org/10.1016/j.engstruct.2020.110414.
[10] Yu J, Luo L, Li Y. Numerical study of progressive collapse resistance of RC beam-slab substructures under perimeter column removal scenarios. Eng Struct 2018;159:14–27. https://doi.org/10.1016/j.engstruct.2017.12.038.
[11] Ghali A, Tadros G. Bridge progressive collapse vulnerability. J Struct Eng 1997;123:227–31. https://doi.org/10.1061/(ASCE)0733-9445(1997)123:2(227).
[12] Wang MR, Zhou ZJ. Progressive collapse and structural robustness of bridges. Appl Mech Mater 2012;193–194:1021–4. https://doi.org/10.4028/www.scientific.net/AMM.193-194.1021.
[13] Jiang H, Wang J, Chorzepa MG, Zhao J. Numerical investigation of progressive collapse of a multispan continuous bridge subjected to vessel collision. J Bridg Eng 2017;22:04017008. https://doi.org/10.1061/(ASCE)BE.1943-5592.0001037.
[14] Starossek U. Avoiding disproportionate collapse of major bridges. Struct Eng Int 2009;19:289–97. https://doi.org/10.2749/101686609788957838.
[15] Bontempi F. Elementary concepts of structural robustness of bridges and viaducts. J Civ Struct Heal Monit 2019;9:703–17. https://doi.org/10.1007/s13349-019-00362-7.
[16] Buitrago M, Bertolesi E, Calderón PA, Adam JM. Robustness of steel truss bridges: laboratory testing of a full-scale 21-metre bridge span. Structures 2021;29:691–700. https://doi.org/10.1016/j.istruc.2020.12.005.
[17] Olmati P, Brando F, Gkoumas K. Robustness assessment of a steel truss bridge. Struct. Congr., Reston, VA: American Society of Civil Engineers; 2013, p. 250–61. https://doi.org/10.1061/9780784412848.023.
[18] Sangiorgio V, Nettis A, Uva G, Pellegrino F, Varum H, Adam JM. Analytical Fault Tree and Diagnostic Aids for the Preservation of Historical Steel Truss Bridges. Eng Fail Anal 2022;133:105996.
[19] DoD. Department of Defense. Design of buildings to resist progressive collapse (UFC 4-023-03); 2009.
[20] GSA. Alternate path analysis & design guidelines for progressive collapse resistance 2013.
[21] EN 1991-1-7. Eurocode 1: Actions on structures - Part 1-7: General actions - Accidental actions; 2006.
[22] Bertolesi E, Buitrago M, Adam JM, Calderón PA. Fatigue Assessment of Steel Riveted Railway Bridges: Full-Scale Tests and Analytical Approach. J Constr Steel Res 2021;182:106664. https://doi.org/10.1016/j.jcsr.2021.106664.
[23] Ivorra S, Buitrago M, Bertolesi E, Torres B, Bru D. Dynamic identification on an ancient steel bridge of six spans. In: Gattulli V, Bursi O, Zonta D, editors. 14th Int. Work. Adv. Smart Mater. Smart Struct. Technol., Rome: Sapienza. Università Editrice; 2019, p. 139–42. https://doi.org/10.13133/9788893771146.
[24] ABAQUS. Abaqus, Theory manual 2019.
[25] Zenzen R, Belaidi I, Khatir S, Abdel WM. A damage identification technique for beam-like and truss structures based on FRF and Bat Algorithm. Comptes Rendus Mec 2018;346:1253–66. https://doi.org/10.1016/j.crme.2018.09.003.
[26] Anitori G, Casas JR, Ghosn M. Redundancy and Robustness in the Design and Evaluation of Bridges: European and North American Perspectives. J Bridg Eng 2013;18:1241–51. https://doi.org/10.1061/(asce)be.1943-5592.0000545.
[27] Xu G, Ellingwood BR. Probabilistic Robustness Assessment of Pre-Northridge Steel Moment Resisting Frames. J Struct Eng 2011;137:925–34. https://doi.org/10.1061/(asce)st.1943-541x.0000403.
[28] Ghosn M, Yang J, Beal D, Sivakumar B, editors. Bridge System Safety and Redundancy. Washington, D.C.: Transportation Research Board; 2014.
[29] Starossek U. Progressive Collapse of Structures. Second Edi. London: ICE Publishing; 2018.
[30] Frangopol DM, Curley JP. Effects of damage and redundancy on structural reliability. J Struct Eng 1987;113(7):1533–49.
[31] Olmati P, Gkoumas K, Brando F, Cao L. Consequence-based robustness assessment of a steel truss bridge. Steel Compos Struct 2013;14:379–95. https://doi.org/10.12989/scs.2013.14.4.379.
[32] Norma Adif Vía (NAV) 3-4-3.0. Montaje de vía en balasto para obra nueva. 2015.
[33] Norma Adif Vía (NAV) 7-1-9.1. Montaje y recepción de la superestructura de vía sin balasto sobre bloques prefabricados. 2001.
[34] Porcu MC, Patteri DM, Melis S, Aymerich F. Effectiveness of the FRF curvature technique for structural health monitoring. Constr Build Mater 2019;226:173–87. https://doi.org/10.1016/j.conbuildmat.2019.07.123.